AMERICAN SOCIETY FOR MICROBIOLOGY | Infection and Immunity®

CELLULAR MICROBIOLOGY:
PATHOGEN-HOST CELL MOLECULAR INTERACTIONS

Temporal Manipulation of Mitochondrial Function by Virulent *Francisella tularensis* To Limit Inflammation and Control Cell Death

Forrest Jessop,[a] Benjamin Schwarz,[a] Emily Heitmann,[a] Robert Buntyn,[a] Tara Wehrly,[a] Catharine M. Bosio[a]

[a]Immunity to Pulmonary Pathogens Section, Laboratory of Bacteriology, Rocky Mountain Laboratories, National Institute of Allergy and Infectious Diseases, National Institutes of Health, Hamilton, Montana, USA

ABSTRACT *Francisella tularensis* subsp. *tularensis* is a highly pathogenic intracellular bacterium that suppresses host inflammation by impairing the metabolic shift from oxidative phosphorylation to glycolysis. Decreased mitochondrial metabolism is central to initiating a metabolic shift to glycolysis and regulating inflammation, but *F. tularensis* subsp. *tularensis* manipulation of host mitochondrial function has not been explored. We demonstrate, using extracellular flux analysis, that *F. tularensis* subsp. *tularensis* infection initially improves host macrophage mitochondrial bioenergetics in a capsule-dependent manner. Enhancement of mitochondrial function by *F. tularensis* subsp. *tularensis* allowed for modest replication and inhibition of apoptosis early after infection. However, using live cell imaging, we found that *F. tularensis* subsp. *tularensis* facilitated the loss of mitochondrial function at later time points during infection in a capsule-independent fashion. This loss of function was paired with oncosis and rapid bacterial replication. Inhibition of oncosis reduced intracellular bacterial numbers, underscoring the requirement for this process during *F. tularensis* subsp. *tularensis* infection. These findings establish that temporal mitochondrial manipulation by *F. tularensis* subsp. *tularensis* is critical for maintenance of a noninflammatory environment and subsequently aids in optimal replication and dissemination of this pathogenic organism.

KEYWORDS *Francisella*, macrophages, metabolism, mitochondria, oncosis

Infection with as few as 10 CFU of *Francisella tularensis* subsp. *tularensis* bacteria can result in the life-threatening disease known as tularemia. Pneumonic acquisition is the most lethal route of infection, resulting in mortality rates approaching 60% (1). Historically, the low infectious dose and high mortality rate led to the development of *F. tularensis* subsp. *tularensis* as a biological weapon and, more recently, its classification as a tier 1 select agent by the Centers for Disease Control and Prevention in the United States. As a facultative intracytosolic pathogen, *F. tularensis* subsp. *tularensis* primarily targets macrophages and dendritic cells for infection and replication. Successful infection with *F. tularensis* subsp. *tularensis* is dependent upon effective suppression and evasion of macrophage activation and the associated inflammation. *F. tularensis* subsp. *tularensis* rapidly impairs host macrophage inflammatory cascades upon contact and is able to replicate to high titers within the cytosolic compartment without triggering cell activation or an overt inflammatory response (2–4). Moreover, cytokine responses are typically delayed until host mortality is imminent (2–4). Therefore, understanding the mechanisms by which *F. tularensis* subsp. *tularensis* manipulates host inflammatory responses is essential for developing novel therapeutics and vaccines.

There is growing recognition of the importance of host cell metabolism in regulating inflammation. A metabolic shift from oxidative phosphorylation (OXPHOS) to aerobic glycolysis is required for macrophage activation and inflammatory cytokine production (5). Metabolites from glycolysis regulate multiple pathways that constitute

Received 17 January 2018 **Returned for modification** 21 February 2018 **Accepted** 9 May 2018

Accepted manuscript posted online 14 May 2018

Citation Jessop F, Schwarz B, Heitmann E, Buntyn R, Wehrly T, Bosio CM. 2018. Temporal manipulation of mitochondrial function by virulent *Francisella tularensis* to limit inflammation and control cell death. Infect Immun 86:e00044-18. https://doi.org/10.1128/IAI.00044-18.

Editor Craig R. Roy, Yale University School of Medicine

Address correspondence to Catharine M. Bosio, bosioc@niaid.nih.gov.

macrophage activation and provide important carbon mass for generation of cytokines and chemokines (5). With an increased reliance on glycolysis for ATP, mitochondria can become repurposed for generation of reactive oxygen species (ROS) and antimicrobial metabolites. Furthermore, the integrity of mitochondria is central to mediating the fate of infected cells, including preservation of viability or activation of programmed death pathways (6). We previously established that the O-antigen polysaccharide capsule of *F. tularensis* subsp. *tularensis* has an integral role in the suppression of host cell inflammatory responses by impairing the metabolic shift to glycolysis (7). However, the specific mechanisms by which *F. tularensis* subsp. *tularensis* and its associated capsule manipulate host cell metabolism, including effects on mitochondrial function, have not been determined.

Herein we provide evidence for the temporal manipulation of mitochondrial function by *F. tularensis* subsp. *tularensis* during infection in two distinct phases. *F. tularensis* subsp. *tularensis* infection initially improves mitochondrial function in a capsule-dependent manner through specific complexes of the electron transport chain (ETC) to promote cell survival and prevent induction of inflammatory responses. Using live cell imaging, we also establish that this first phase of infection is followed by rapid dissolution of the mitochondrial potential, resulting in dramatic oncotic events that are independent of capsule. Furthermore, the loss of mitochondrial function and oncosis were required for optimal bacterial replication. Our data provide novel insight into how a highly pathogenic, intracellular pathogen manipulates the host cell metabolism to initially temper inflammatory responses followed by rapid replication and points to new targets that could be exploited by novel antimicrobial therapeutics.

RESULTS

***F. tularensis* subsp. *tularensis* capsule manipulates host mitochondrial function.** A metabolic shift from OXPHOS to glycolysis is essential for activation of macrophages and repurposing the mitochondria as a proinflammatory signaling platform (5). Prior studies in our laboratory demonstrated an integral role for *F. tularensis* subsp. *tularensis* capsule in preventing host macrophage activation by impairing the metabolic shift to glycolysis following infection (7). However, it was unclear if the capsule directly interfered with steps in the glycolytic pathway or if the inability of the cell to shift to glycolysis was a result of manipulation of mitochondrial function. To determine if *F. tularensis* subsp. *tularensis* capsule affected mitochondrial function, we assessed mitochondrial bioenergetics following infection with *F. tularensis* subsp. *tularensis* (SchuS4) or a *F. tularensis* subsp. *tularensis* capsule mutant, SchuS4 Δ1238 (Δ1238). Both bacteria and host cells undergo respiration in culture. Thus, before we could determine the impact of *F. tularensis* subsp. *tularensis* infection on host cell mitochondrial function, we established the threshold of bacterial numbers that may contribute to our readout for this organelle, i.e., oxygen consumption. Increasing numbers of SchuS4 bacteria were suspended in Seahorse Mito Stress medium (nutrient minimal) or modified Mueller-Hinton (MMH) broth (a nutrient-rich broth used to propagate *F. tularensis* subsp. *tularensis*), and the oxygen consumption rates (OCR) were assessed as previously described for other bacterial pathogens (8). As expected, OCR increased proportionally with the number of bacteria. However, OCR was greater in MMH broth than in Seahorse Mito Stress medium (see Fig. S1A in the supplemental material). The limit of detection of OCR by SchuS4 was approximately 500,000 CFU in both media. Therefore, we utilized multiplicities of infection (MOIs) and time points after infection in which the number of bacteria within host cells was below this threshold (3 to 9 h; Fig. S1B) for the following experiments.

Next, we measured mitochondrial function among infected bone marrow-derived macrophages (BMM) in real time following injection of oligomycin A, carbonyl cyanide-*p*-trifluoromethoxyphenylhydrazone (FCCP), and rotenone-antimycin, as detailed in Fig. S2. Infection with either SchuS4 and Δ1238 resulted in increased basal mitochondrial respiration rates and proton leak among host cells as early as 6 h after infection (Fig. 1A to C). In contrast, SchuS4 infection resulted in maintenance of spare respiratory

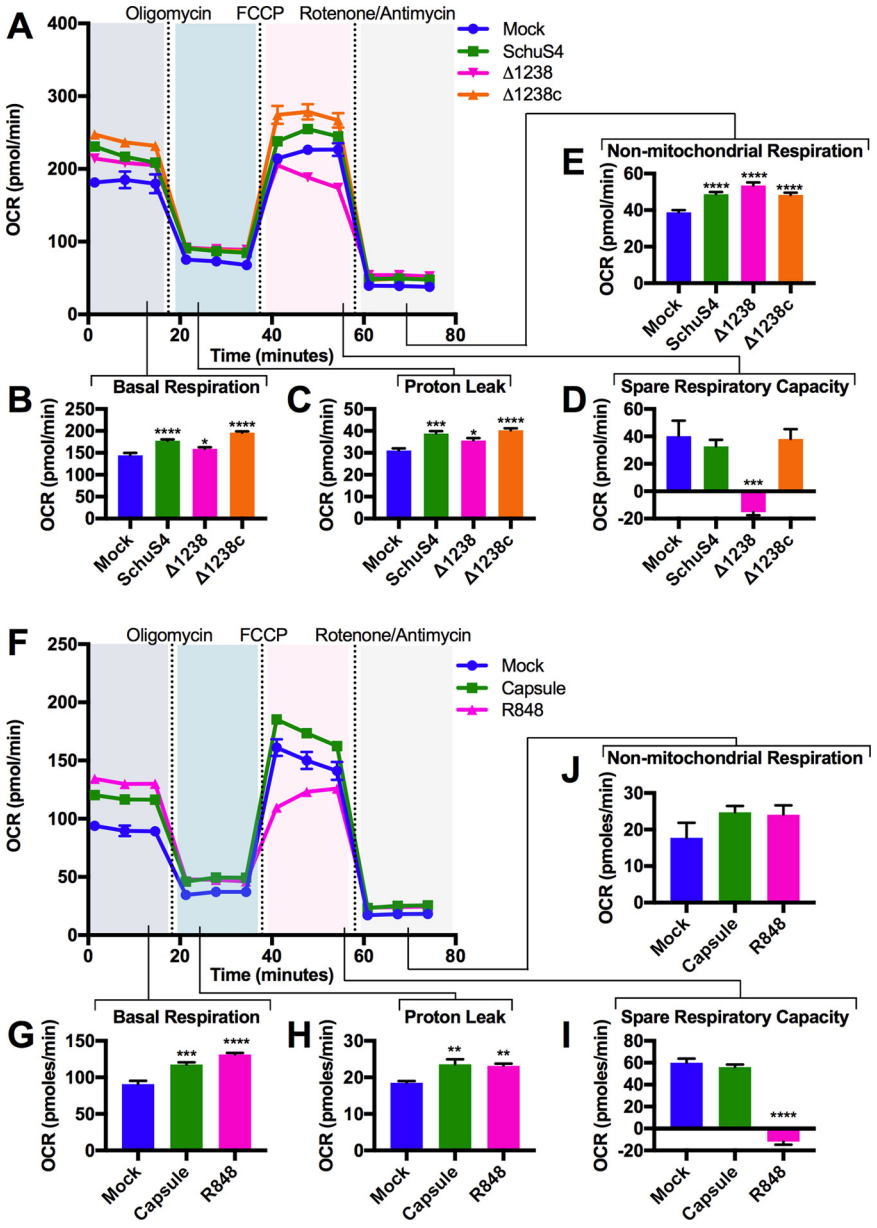

FIG 1 *F. tularensis* subsp. *tularensis* capsule manipulates host mitochondrial function. (A) Results of the Mito Stress test performed on BMM at 6 h following infection with SchuS4, Δ1238, or Δ1238c (MOI, 50). (B to E) Individual parameters of mitochondrial function were obtained from the trace in panel A, including basal respiration (B), proton leak (C), spare respiratory capacity (D), and nonmitochondrial respiration (E). (F) Results of the Mito Stress test on BMM at 6 h following treatment with isolated capsule (10 μg/ml) or R848 (5 ng/ml). (G to J) Individual parameters of mitochondrial function were obtained from the trace in panel F, including basal respiration (G), proton leak (H), spare respiratory capacity (I), and nonmitochondrial respiration (J). Metabolic traces from a representative experiment that was repeated 3 times with similar results are shown. Data are presented as the mean ± SEM for 6 technical replicates. *P* values were determined using one-way ANOVA. *, $P < 0.05$; **, $P < 0.01$; ***, $P < 0.001$; ****, $P < 0.0001$.

capacity, while infection with Δ1238 decreased this parameter compared to that in mock-infected cells (Fig. 1D). No significant differences in nonmitochondrial respiration rates were observed between SchuS4 and Δ1238 (Fig. 1E). The SchuS4 Δ1238 complemented mutant (Δ1238c) behaved similarly to SchuS4, confirming the role of capsule in manipulation of mitochondrial function (Fig. 1A to E). The ability of SchuS4 to increase basal respiration while maintaining spare respiratory capacity is consistent with the hypothesis that SchuS4 improves mitochondrial function, in part, through a capsule-dependent process.

We next confirmed that capsule had a direct role in increased host cell mitochondrial metabolism. Similar to the findings after infection with intact SchuS4, addition of purified SchuS4 capsule to BMM resulted in increased basal respiration and proton leak and maintained the spare respiratory capacity at 6 h posttreatment compared to that in cells treated with the Toll-like receptor 7 (TLR7)/TLR8 agonist R848 or mock-treated controls (Fig. 1F to I). Both R848 and capsule marginally increased nonmitochondrial respiration rates (Fig. 1J). The increased mitochondrial basal respiration and sustained spare respiratory capacity were dose dependent (Fig. S3A and B) and maintained for up to 24 h after treatment (data not shown). To determine if the effects of SchuS4 capsule on mitochondrial function were a general feature of exposure to complex bacterial capsules, we examined the ability of *Klebsiella pneumoniae* capsule to manipulate mitochondrial function and glycolysis. In contrast to SchuS4 capsule, *K. pneumoniae* capsule stimulated a shift away from OXPHOS to glycolysis and drove cytokine production, whereas SchuS4 capsule did not induce glycolysis or cytokine responses (Fig. S4A to C). Together these data support the notion that SchuS4 capsule contributes to the increased function of mitochondria among *F. tularensis* subsp. *tularensis*-infected cells and that capsule is unique in its ability to maintain mitochondrial function compared to another complex polysaccharide capsule.

SchuS4 improves mitochondrial metabolism through ETC complexes I and II. The electron transport chain (ETC) is the heart of the mitochondria, transferring electrons and protons and coupling with OXPHOS for the generation of ATP. The ability of SchuS4 to increase basal respiration and maintain spare respiratory capacity may reflect altered ETC activity. To address this question, we permeabilized SchuS4-infected BMM and directly supplied mitochondria with specific complex I or II substrates following methods adapted from those of Divakaruni et al. (9). Permeabilization of host cells allowed for quantification of state 3 respiration (phosphorylating respiration that is controlled by substrate oxidation and ATP synthase activity), state 4o respiration (unphosphorylating respiration that is indicative of proton leak), and the respiratory control ratio (RCR; calculated as the state 3 OCR/state 4o OCR). The RCR is used as an overall indicator of mitochondrial health (10). SchuS4 infection increased state 3 respiration rates in the presence of glutamate and fatty acids (complex I) and succinate (complex II) (Fig. 2A). No significant differences in state 3 respiration rates were observed between mock- and SchuS4-infected cells provided with pyruvate (complex I) (Fig. 2A). This suggested that SchuS4 increased mitochondrial respiration rates via manipulation of both complex I and II in a manner that did not require increased pyruvate utilization. In contrast, infection with Δ1238 resulted in decreased state 3 respiration rates when pyruvate, glutamate, and fatty acid were supplied to the mitochondria (Fig. 2A). The capsule complement mutant (Δ1238c) increased state 3 respiration rates when glutamate and fatty acid were supplied to the mitochondria, similar to the findings for SchuS4 (Fig. 2A). SchuS4, Δ1238, and Δ1238c infection increased state 4o respiration rates, and these rates were not significantly different from each other, indicating that *F. tularensis* subsp. *tularensis* infection caused an increased proton leak that was independent of capsule (Fig. 2B). Finally, SchuS4- and Δ1238c-infected BMM had significantly higher RCR values than Δ1238-infected BMM (Fig. 2C). Taken together, these data indicate that the increase and/or maintenance of complex I and II activity and the concomitant maintenance of mitochondrial ETC function early after SchuS4 infection are capsule dependent.

To further confirm the contribution of capsule to improvement of mitochondrial ETC function, we next exposed BMM to isolated capsule and assessed substrate utilization by specific ETC complexes, as described above. The findings obtained with BMM treated with capsule recapitulated the findings observed among SchuS4-infected cells, including a general increase in complex I and II substrate utilization (Fig. 2D). However, with capsule exposure, a significant increase in pyruvate utilization was also observed. BMM treated with capsule also had increased state 4o respiration rates when glutamate and succinate were supplied to the mitochondria. No significant differences from the results obtained with the other complex I substrates were observed, though a trend

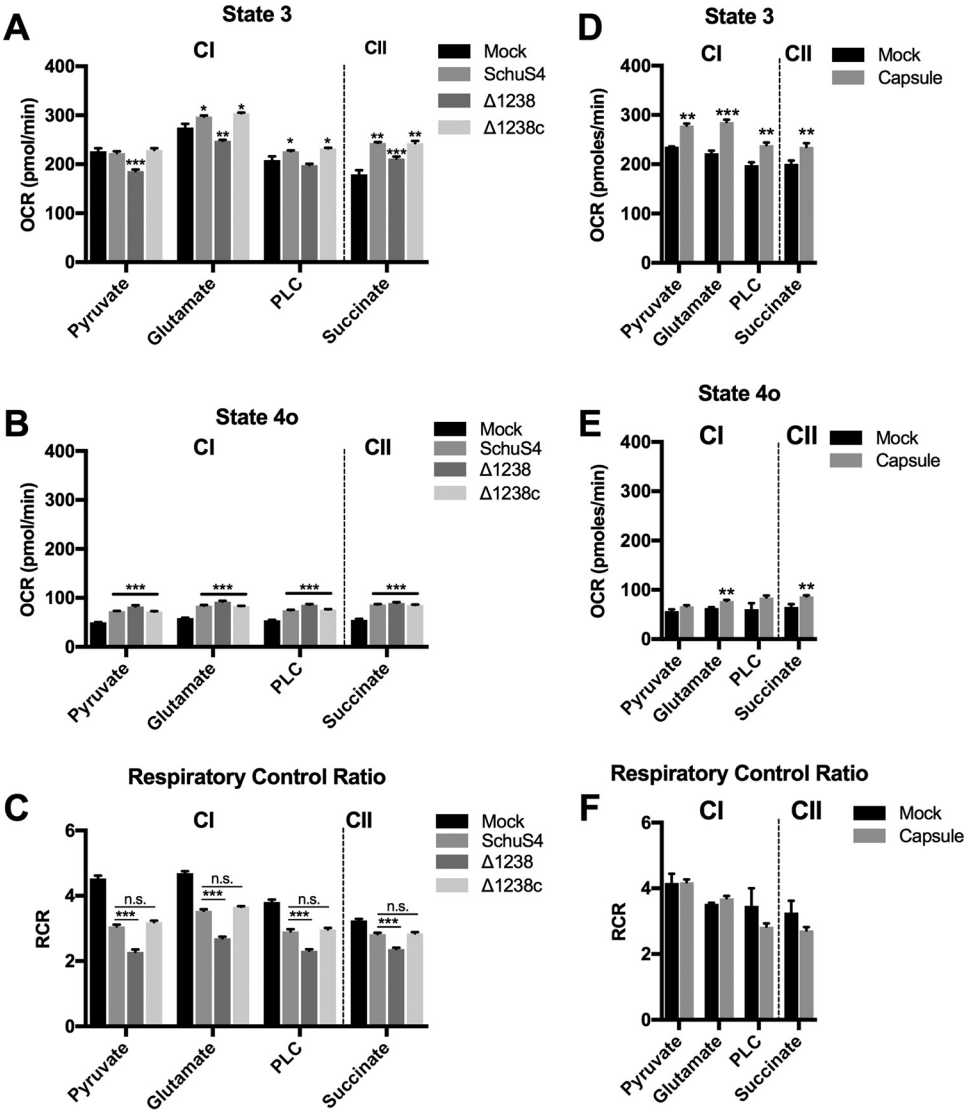

FIG 2 SchuS4 improves mitochondrial metabolism through ETC complex I (CI) and complex II (CII). (A) State 3 respiration rates for the complex I substrates pyruvate, glutamate, and palmitoyl-L-carnitine (PLC) and the complex II substrate succinate at 6 h following SchuS4, Δ1238, or Δ1238c infection (MOI, 50). (B) State 4o respiration rates following oligomycin injection (2 μM) for complex I substrates pyruvate, glutamate, and palmitoyl-L-carnitine and complex II substrate succinate at 6 h following SchuS4, Δ1238, or Δ1238c infection (MOI, 50). (C) The corresponding respiratory control ratio (RCR; state 3 OCR/state 4o OCR) from panels A and B. (D) State 3 respiration rates for complex I substrates pyruvate, glutamate, and palmitoyl-L-carnitine and complex II substrate succinate at 6 h following treatment of BMM with isolated SchuS4 capsule (10 μg/ml). (E) State 4o respiration rates following oligomycin injection (2 μM) for complex I substrates pyruvate, glutamate, and palmitoyl-L-carnitine and complex II substrate succinate at 6 h following treatment of BMM with isolated SchuS4 capsule (10 μg/ml). (F) The corresponding RCR from panels D and E. Data from a representative experiment that was repeated 3 times with similar results are shown. Data are presented as the mean ± SEM for 6 to 8 technical replicates. *P* values indicate the significance of the difference compared to the mock-infected group or the indicated group, determined using one-way ANOVA. n.s., not significant; *, $P < 0.05$; **, $P < 0.01$; ***, $P < 0.001$.

toward increased proton leak was evident (Fig. 2E). Finally, no significant differences in RCR were observed between mock- and capsule-treated BMM (Fig. 2F). This is likely due to no significant change in the magnitude of state 4o respiration rates following capsule treatment. Together, these data demonstrate that there was both capsule-dependent and -independent manipulation of the mitochondria by SchuS4. Specifically, the general increase in mitochondrial ETC function through both complex I and II substrate utilization and maintenance of complex I activity was capsule dependent, whereas the proton leak triggered by *F. tularensis* subsp. *tularensis* was independent of capsule.

Capsule increases mitochondrial network volume. The increased mitochondrial respiration following SchuS4 infection or capsule treatment may reflect changes in mitochondrial morphology, number, or size. Thus, we next evaluated if SchuS4-mediated enhancements of mitochondrial function were associated with alterations in any of these parameters. We did not observe any significant differences in mitochondrial DNA (mtDNA) copy number between infected and mock-infected BMM, indicating that mitochondrial biogenesis was not a major factor contributing to increased OCR following infection (Fig. 3A and B). No significant differences in cytochrome *c* levels were observed following SchuS4 infection (Fig. 3C and D). However, increased cytochrome *c* levels were observed following exposure to capsule (Fig. 3E and F), suggesting that mitochondrial size or content may be altered. An alteration in cytochrome *c* levels may not reflect changes in mitochondrial morphology, such as fusion of mitochondrial networks, that can result in increased respiration rates (11). To assess mitochondrial network or volume expansion, BMM were infected with SchuS4 or treated with capsule and then stained after 6 h using MitoTracker Red. z-stack images were acquired, and mitochondrial networks were modeled in three dimensions (3D) using Imaris software, allowing determination of the mitochondrial network volume relative to the total cell volume. Both SchuS4 infection and capsule treatment increased the mitochondrial network volume (Fig. 3G to J). Taken together, these findings suggest that increased OXPHOS following capsule exposure correlates with increased mitochondrial network volume.

SchuS4 and capsule impair apoptotic cell death. We previously established that SchuS4 inhibits glycolysis, and data presented herein suggest that this is a feature of its ability to enhance mitochondrial function as a mechanism to limit production of proinflammatory cytokines (7). However, manipulation of mitochondrial activity and morphology early during SchuS4 infection may also serve to prevent apoptosis (11) and thereby maintain the replicative niche of this intracellular bacterium. To test this hypothesis, we utilized multiple mechanisms to induce intrinsic apoptosis in BMM infected with SchuS4 or treated with capsule. Removal of macrophage colony-stimulating factor (M-CSF) from primary cells has been shown to induce apoptosis through mitochondrial membrane destabilization, resulting in activation of caspase-9 (12). Therefore, we infected cells with SchuS4 and deprived cultures of M-CSF for 48 h to determine if SchuS4 impaired apoptosis under M-CSF-depleted conditions. BMM infected with SchuS4 displayed significantly less cell death following removal of M-CSF from cultures than mock-infected controls (Fig. 4A). Similarly, BMM treated with SchuS4 capsule also had significantly less cell death than mock-treated cells when M-CSF was removed from the cultures (Fig. 4B). We confirmed these results by microscopy using the vital dye NucGreen. Both SchuS4 and capsule significantly reduced the number of NucGreen-positive cells in M-CSF-depleted cultures (Fig. 4C and D).

Increased amounts of cleaved caspase-9 and caspase-3 are central indicators of mitochondrion-associated apoptosis. In agreement with the reduction in cellular cytotoxicity observed as described above, SchuS4-infected and capsule-treated cells had reduced cleaved caspase-9 and caspase-3 compared to mock-infected BMM depleted of M-CSF (Fig. 4E to H). Staurosporine (STS) treatment of BMM for 9 h was used as an additional positive control for induction of apoptosis. These data indicate that *F. tularensis* subsp. *tularensis* and its associate capsule suppressed the progression of cells toward apoptosis. To further confirm a role for manipulation of mitochondrion-directed apoptosis, we tested the ability of SchuS4 and capsule to impair cytotoxicity in BMM following treatment with the complex I inhibitor rotenone. Both SchuS4 infection and capsule treatment significantly inhibited rotenone-induced cell death (Fig. 4I to J). Therefore, in addition to limiting inflammatory responses, amplification of mitochondrial activity by SchuS4 also aids in resistance to induction of apoptosis among infected cells.

SchuS4 capsule-independent transition to prooncotic phase of cell death. Although we established that SchuS4 actively inhibits apoptosis, eventually, infected

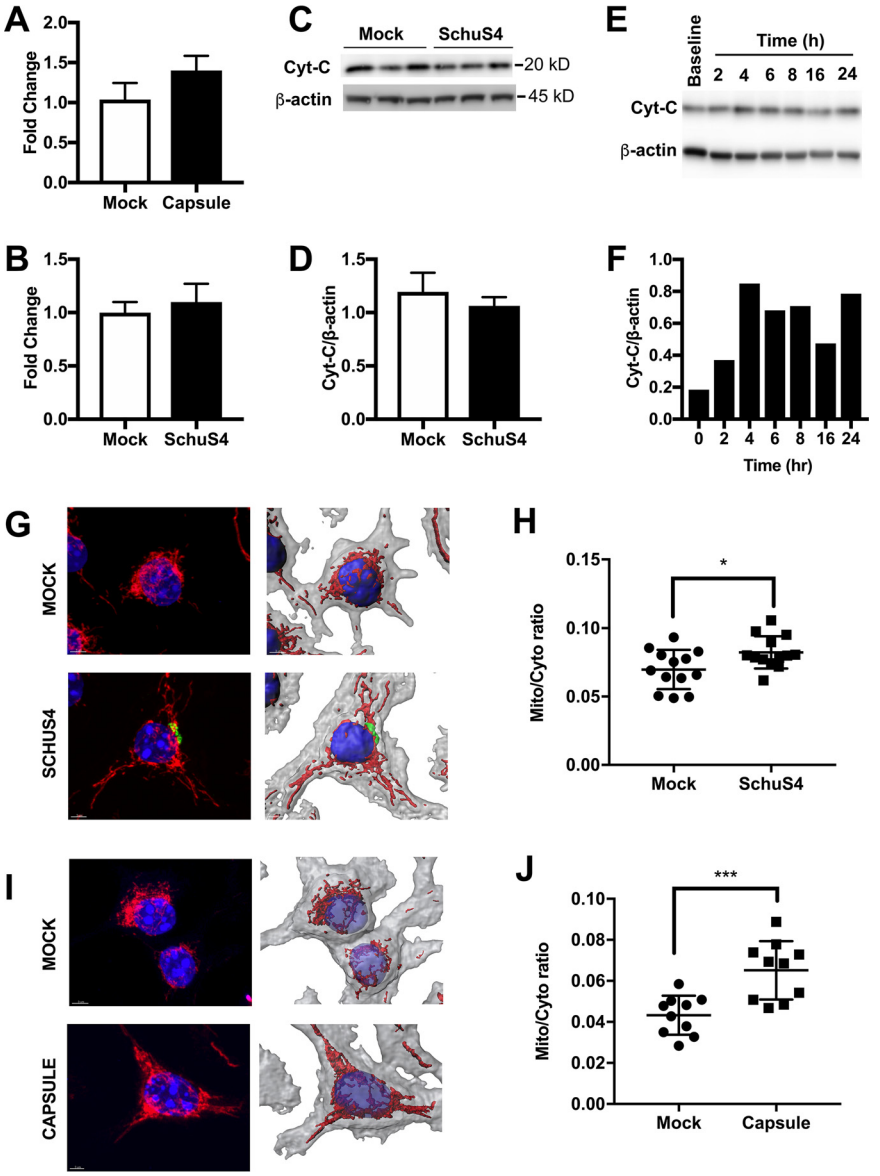

FIG 3 Capsule increases mitochondrial network volume. (A) Mitochondrial DNA copy number at 6 h following SchuS4 infection (MOI, 50). (B) Mitochondrial DNA copy number at 6 h following capsule treatment (10 μg/ml). (C and D) Western blot of cytochrome *c* (Cyt-C) (C) and the corresponding densitometry of cytochrome *c* levels (D) in BMM cell lysates at 6 h following SchuS4 infection (MOI, 50). (E and F) Western blot of cytochrome *c* (E) and the corresponding densitometry of cytochrome *c* levels (F) in BMM cell lysates over time following capsule treatment (10 μg/ml). (G) MitoTracker Red staining and Imaris 3D reconstruction of the mitochondrial network in BMM at 6 h after SchuS4 infection (MOI, 50). (H) The corresponding quantification of the mitochondrial network volume from panel G. Mito/Cyto, MitoTracker Red volume/cytosolic volume ratio. (I) MitoTracker Red staining and Imaris 3D reconstruction of the mitochondrial network in BMM at 24 h after treatment with capsule (10 μg/ml). (J) The corresponding quantification of the mitochondrial network volume from panel I. Western blot images and densitometry results are representative of those from 3 separate experiments. Confocal images are representative of those from 2 separate experiments in which 10 to 12 cells were used per group for 3D reconstruction and quantification of the mitochondrial network volume. For quantification of the mitochondrial volume and mtDNA copy number, data are presented as the mean ± SEM (three technical replicates) from one representative experiment which was repeated three times. *P* values were determined using Student's *t* test. *, $P < 0.05$; ***, $P < 0.001$.

cells do die. How this process occurs in SchuS4-infected macrophages, including the discrete sequence of events, is not understood. It has been shown that attenuated strains of *Francisella* induce either pyroptosis or necroptosis (13–16). We have previously shown that SchuS4 does not induce inflammasome activity and associated

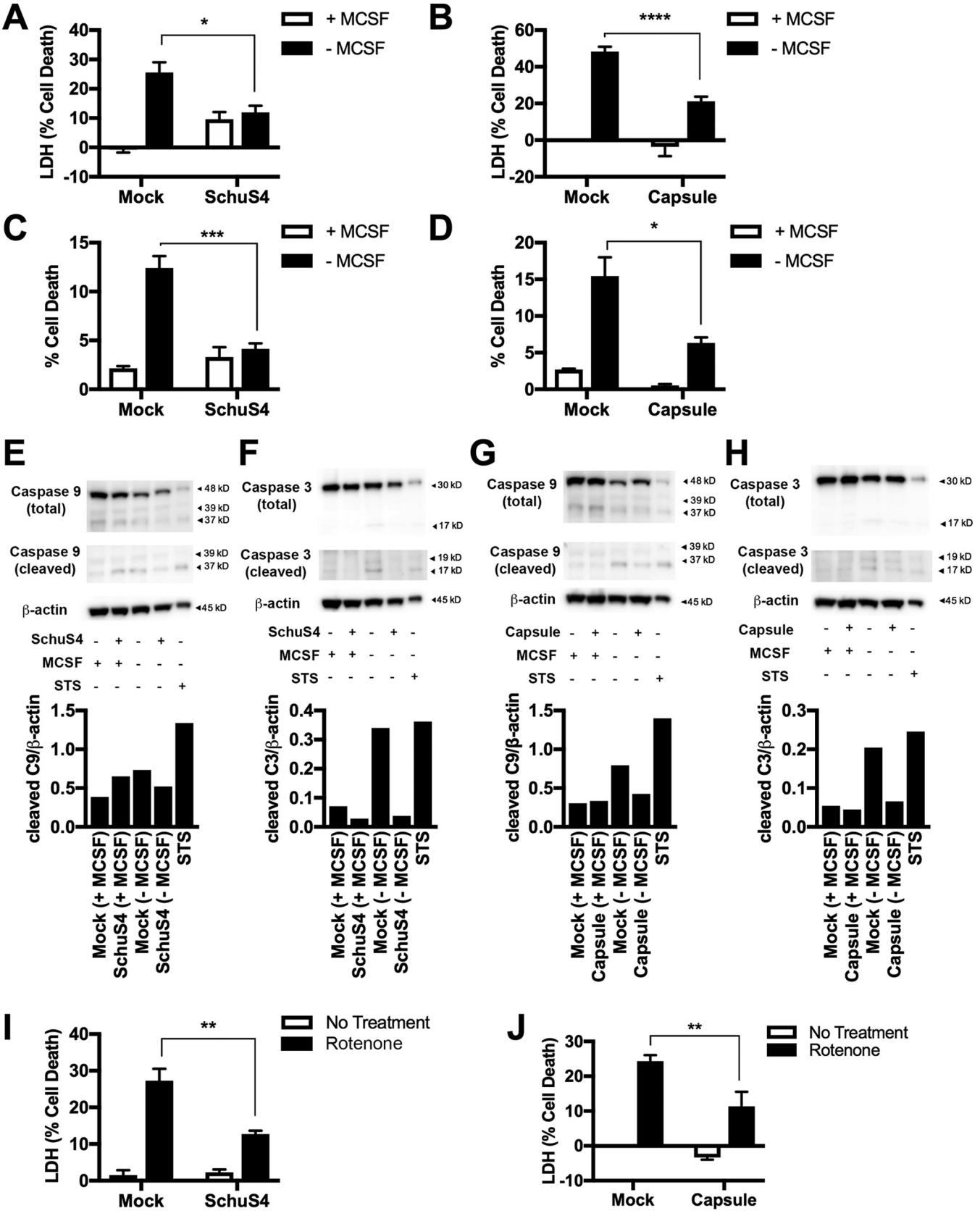

FIG 4 SchuS4 and capsule impair apoptotic cell death. (A) Cytotoxicity, as determined by extracellular LDH activity, in BMM infected with SchuS4 (MOI, 5) and then starved of M-CSF (48 h). (B) Cytotoxicity, as determined by extracellular LDH activity, in BMM exposed to capsule (10 μg/ml) and then starved of M-CSF (48 h). (C) Percent cell death, as determined by the percentage of NucGreen-positive cells, in BMM infected with SchuS4 (MOI, 5) and then starved of M-CSF

(Continued on next page)

pyroptosis (17). Necroptosis is a form of programmed cell death that is also linked to mitochondrial health. A recent report indicated that attenuated *F. tularensis* subsp. *holarctica* (LVS) promoted mitochondrial failure and necroptosis in BMM, as measured by an increase in phosphorylated receptor-interacting protein kinases (RIPK) and mixed-lineage kinase domain-like pseudokinase (MLKL) (16). Given the ability of SchuS4 to modulate mitochondrial function, we determined if SchuS4 induced necroptosis in BMM, as is similarly observed among cells infected with LVS. Tumor necrosis factor alpha (TNF-α), in addition to the pan-caspase inhibitor Z-Val-Ala-Asp fluoromethyl ketone (ZVAD), was used as a positive control for induction of the phosphorylation of MLKL required for necroptosis (Fig. S5A and B). In agreement with previously published results, BMM infected with LVS triggered increased phosphorylation of RIPK and MLKL in a dose- and time-dependent manner (Fig. S5C to F) (16). However, cytotoxicity was not significantly different between LVS-infected BMM and LVS-infected BMM treated with necrostatin-1 (Fig. S5G). Furthermore, necrostatin-1 treatment of LVS-infected cells did not significantly impair bacterial replication (data not shown). Discrepancies in our results with LVS and those with LVS previously published may be a consequence of the different infection models used between the studies (16). Regardless, in contrast to LVS, SchuS4 infection of BMM resulted in no change in the amount of phosphorylated RIPK at 24 and 48 h (MOI, 10) and decreased the amount of phosphorylated MLKL compared to that in mock-infected cells over time (Fig. S6A to C). Addition of necrostatin-1 had no significant effect on cell death or bacterial replication among SchuS4-infected cells (Fig. S6D to G). These data indicate that while necroptosis may be a feature of LVS-triggered cell death, it is not a primary mechanism of cell death following SchuS4 infection. The altered capacity of LVS to manipulate mitochondrial function, similar to that of SchuS4, may account for the increased apoptosis or necroptosis. Therefore, we compared the mitochondrial function of SchuS4- and LVS-infected BMM at 6 h. LVS infection increased basal respiration rates more than SchuS4 infection did at 6 h but decreased spare respiratory capacity rates, indicating mitochondrial dysfunction (Fig. S7A to D). Additionally, increases in basal respiration rates were temporally protracted in LVS-infected cultures compared to SchuS4-infected cultures (Fig. S7E), further supporting the notion that LVS interacts with host mitochondria differently than SchuS4.

Since we did not observe cells undergoing apoptosis or necroptosis, it was possible that the mechanism of cell death mediated by SchuS4 was an alternative cell death process. Oncosis is a form of cell death morphologically characterized by cell swelling and blistering (18). Therefore, we determined whether SchuS4 induced oncosis in infected cells. Cell swelling is preceded by a loss in mitochondrial membrane potential ($\Delta\Psi_M$) due to opening of the mitochondrial membrane permeability transition pore (mPTP), resulting in depletion of the ATP needed for maintenance of Na+/K ion pumps. Thus, we first determined if there were temporal changes in ATP levels among SchuS4-infected cells. ATP levels increased at 4 h postinfection, consistent with increased OCR (Fig. 1 and 5A). However, ATP levels decreased back to the levels for mock-infected cells by 8 h and were reduced to below those for mock-infected cells by 24 h and 48 h after infection (Fig. 5A). The drop in ATP at these later time points was not due to significant changes in cytotoxicity compared to that for the mock-infected

FIG 4 Legend (Continued)
(48 h) (D) Percent cell death, as determined by the percentage of NucGreen-positive cells, in BMM exposed to capsule (10 μg/ml) and then starved of M-CSF (48 h). (E) Western blots and the corresponding densitometry analysis results showing cleaved and total caspase-9 (C9) levels in BMM infected with SchuS4 (MOI, 5) and then starved of M-CSF (48 h). Staurosporine treatment (1 μM) of BMM for 9 h was used as the positive control. (F) Western blots and the corresponding densitometry analysis results showing cleaved and total caspase-3 (C3) levels in BMM infected with SchuS4 (MOI, 5) and then starved of M-CSF (48 h). Staurosporine treatment (1 μM) of BMM for 9 h was used as the positive control. (G) Western blots and the corresponding densitometry analysis showing cleaved and total caspase-9 levels in BMM exposed to capsule (10 μg/ml) and then starved of M-CSF (48 h). Staurosporine treatment (1 μM) of BMM for 9 h was used as the positive control. (H) Western blots and the corresponding densitometry analysis showing cleaved and total caspase-3 levels in BMM exposed to capsule (10 μg/ml) and then starved of M-CSF (48 h). Staurosporine treatment (1 μM) of BMM for 9 h was used as the positive control. (I) Extracellular LDH levels in BMM culture supernatants at 24 h following infection with SchuS4 (MOI, 10) and exposure to rotenone (8 μM). (J) Extracellular LDH levels in BMM culture supernatants at 24 h following exposure to capsule (10 μg/ml) and rotenone (8 μM). Western blot images and densitometry results are representative of those from 3 separate experiments. Otherwise, data are presented as the mean $\pm$ SEM (3 technical replicates) from one representative experiment that was repeated 3 times with similar results. *P* values were determined using two-way ANOVA. *, $P < 0.05$; **, $P < 0.01$; ***, $P < 0.001$; ****, $P < 0.0001$.

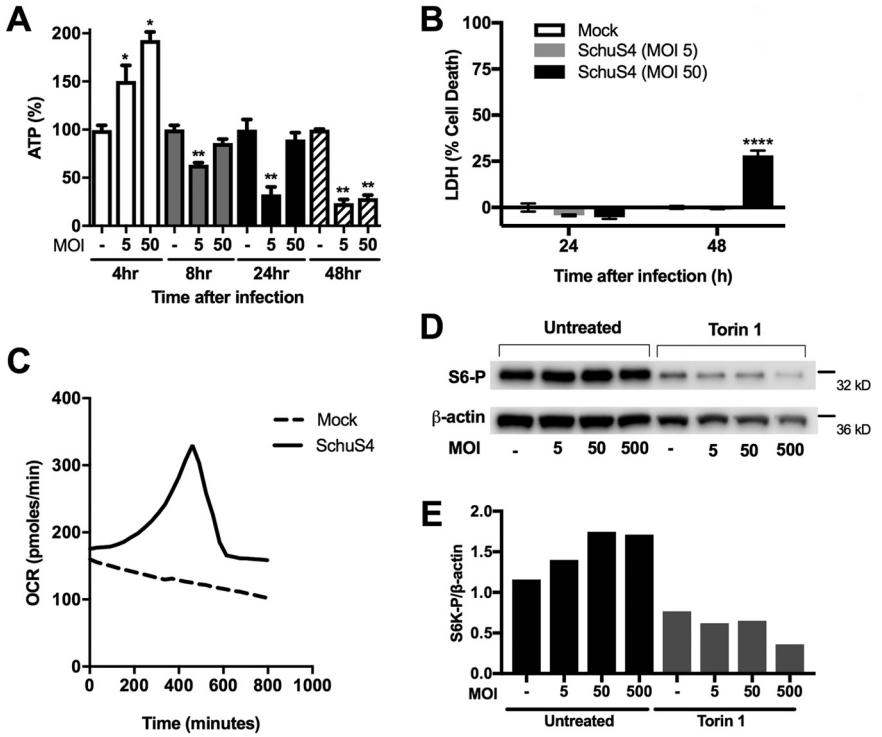

FIG 5 SchuS4 induces the rapid loss of ATP and oxygen consumption and an increase in mTOR activity in BMM, indicative of oncosis. (A) ATP levels in BMM at 4, 8, 24, and 48 h following SchuS4 infection (MOI, 5, 50). (B) LDH assay on mock- and SchuS4-infected macrophages (MOI, 5 and 50) at 24 and 48 h. (C) Real-time trace of basal OCR in mock-infected versus SchuS4-infected macrophages (MOI, 50). (D and E) Representative Western blots (D) and corresponding densitometry analysis (E) of phosphorylated S6K (S6-P) levels in SchuS4-infected BMM (MOI, 5, 50, and 500 at 24 h). Cells were pretreated with Torin-1 (500 nM) or the vehicle as a control. Western blot images and densitometry, OCR traces, and confocal images with the corresponding TMRE fluorescent intensity analysis results are representative of those from 3 separate experiments. Otherwise, data are presented as the mean ± SEM (3 technical replicates) from one representative experiment of three repeats with similar results. *P* values were determined using Student's *t* test. *, $P < 0.05$; **, $P < 0.01$; ****, $P < 0.0001$.

controls (Fig. 5B). We next confirmed if the decrease in ATP correlated with reduced OCR at these later time points after infection. As expected, we observed a decreasing basal OCR among mock-infected cells over time, consistent with a starvation response due to the minimal nutrients available in Seahorse Mito Stress medium. In SchuS4-infected macrophages (MOI, 50), OCR steadily climbed, reaching a maximal level at 7.5 h, and then rapidly dropped back to basal levels by 10 h (Fig. 5C). OCR among SchuS4-infected cells did not fully decline to those observed in mock-infected cells. However, this may have been a consequence of the increased bacterial load and a contribution of microbial metabolism at these late time points of infection. In addition to a drop in ATP, increased mTOR activity has been reported to be a prooncotic signal acting on glycogen synthase kinase-3, which inhibits mPTP opening (19, 20). We observed increased mTOR activity at 24 h following infection at multiple MOIs, as indicated by the increased phosphorylation of the downstream ribosomal target S6K (Fig. 5D and E), consistent with a prooncotic state.

Oncosis is the primary form of cell death following SchuS4 infection. We next determined if SchuS4-infected cells exhibited morphological traits of oncotic cells. For these studies, live cell imaging was used to observe morphological changes among SchuS4-green fluorescent protein (GFP)-infected macrophages in real time. Since oncosis can be triggered by a decreased mitochondrial membrane potential ($\Delta\Psi_M$), cells were stained with tetramethylrhodamine (TMRE) to monitor this parameter. A time-lapse video of BMM cultures following infection with SchuS4-GFP (MOI, 50) showed that infected cells undergo a process of cell death morphologically indicative of oncosis,

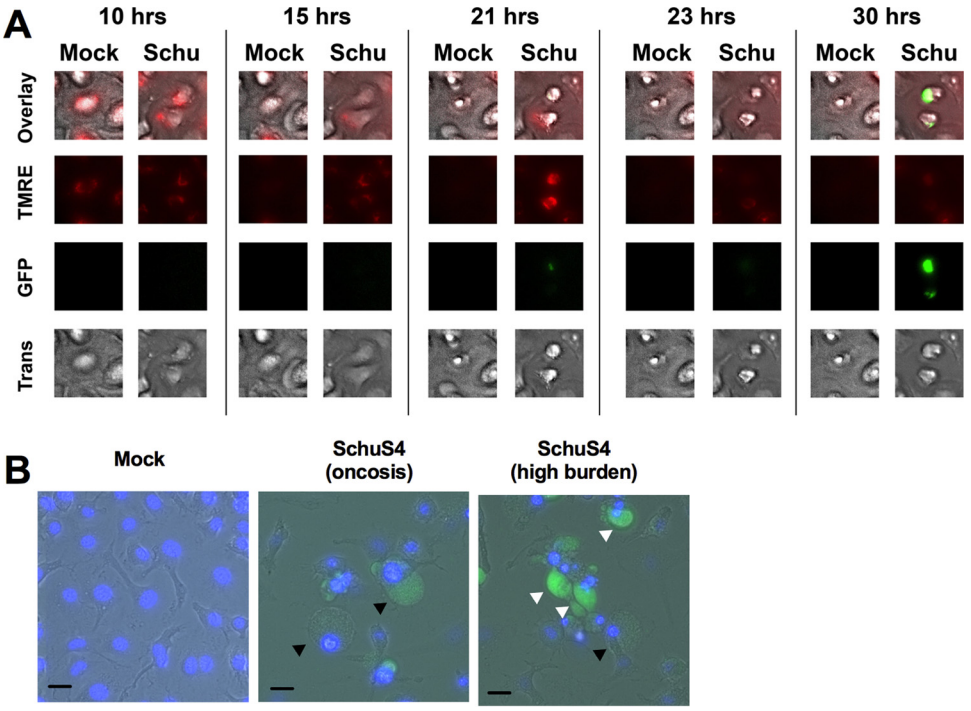

FIG 6 SchuS4 infection causes oncosis as the primary form of cell death. (A) Representative images of a single cell from a time-lapse video (30 h) of mock- and SchuS4-GFP-infected cells. The mitochondrial membrane potential was observed by staining BMM with TMRE. BMM were imaged in the GFP channel to detect the bacterial burden, in the Texas Red channel to detect TMRE, and with transmitted light (Trans) to observe the morphological characteristics of oncosis. (B) Representative images of mock-infected, oncotic, and SchuS4-GFP-laden (postoncosis) macrophages at a higher magnification (×40). Bars, 10 μm. Black arrows point to oncotic cells. White arrows indicate postoncotic cells with high bacterial loads. Cell nuclei were stained using DAPI. The representative images shown were taken from one of three separate experiments with similar results.

including the formation of large cell blisters (mock-infected cells are shown in Video S1, and SchuS4-infected cells are shown in Video S2). Representative frames from a time-lapse video are shown for a single cell in Fig. 6A, though blistering is difficult to observe due to resolution limitations of the membrane. Therefore, higher-resolution live cell images of oncosis following SchuS4 infection are shown in Fig. 6B. In agreement with the depletion of ATP and activation of mTOR, oncosis was immediately proceeded by dramatic mitochondrial depolarization and then the collapse of the mitochondrial network (Video S3; representative frames are shown in Fig. 6A). Interestingly, bacterial replication was significantly enhanced within the cell following oncosis (Video S3; Fig. 6A). Representative live cell images acquired at a higher resolution showing bacterium-laden cells postoncosis are presented in Fig. 6B. Additionally, oncosis occurred in bystander cells that had no to minimal bacterial burden (Videos S2 and S3). In agreement with the relatively noninflammatory nature reported with rapid oncotic cell death (21), we did not detect interleukin-6 (IL-6) or TNF-α at any time after infection (data not shown) and only a minimal amount of IL-12p40 at 72 h postinfection (Fig. S8). Together, these data suggest that SchuS4 promotes an oncotic cell death process via the loss of ATP, increased mTOR activity, and mitochondrial membrane depolarization as a mechanism to rapidly replicate in a noninflammatory environment.

Inhibition of oncosis temporally limits SchuS4 infection. Given the rapid replication of SchuS4 among oncotic cells, we hypothesized that impairing oncotic cell death would both reduce cytotoxicity and limit the bacterial burden in BMM cultures. Torin-1 is a cell-permeant pyridinonequinoline derivative that is a potent inhibitor of mTOR activity. Therefore, addition of this inhibitor may reduce mTOR-dependent cell death processes, such as oncosis, and subsequently impact the intracellular replication

of SchuS4. Torin-1 pretreatment of BMM effectively blocked the increase in mTOR activity induced by SchuS4 (Fig. 5D and E). Torin-1 treatment of SchuS4-infected BMM resulted in a reduction in bacterial numbers at 48 and 72 h after infection at an MOI of 5 and at 48 h after infection at an MOI of 50 (Fig. 7A). No suppression of bacterial replication was observed following infection at an MOI of 500, indicating that enough bacteria can overcome the inhibitory response of this drug. Torin-1 treatment of SchuS4-infected macrophages also decreased SchuS4-induced cytotoxicity in a time- and MOI-dependent manner (Fig. 7B). Importantly, Torin-1 did not directly impair bacterial replication in MMH growth medium or tissue culture medium at the doses used in these studies, suggesting that the effect of this inhibitor on SchuS4 replication was due to manipulation of host cell components (Fig. S9A and B). mTOR is involved in a variety of pathways in host cell metabolism; thus, it was important to compare the control of SchuS4 replication with an additional drug that more directly targeted mitochondria. Cyclosporine impairs mPTP opening and mitochondrial depolarization and limits oncotic events in treated cells (22, 23). Thus, we examined the effect of cyclosporine on SchuS4-infected BMM. We first confirmed that cyclosporine did not directly impair bacterial replication in MMH growth medium (Fig. S9C and D). Similar to the effect of inhibiting mTOR, treatment of infected BMM with cyclosporine significantly reduced the bacterial burden at between 24 and 48 h among cells infected at an MOI of 5 or 50 (Fig. 7C). Cyclosporine treatment of SchuS4-infected macrophages decreased SchuS4-induced cytotoxicity in a time- and MOI-dependent manner (Fig. 7D).

We next confirmed that treatment of BMM with Torin-1 and cyclosporine to limit SchuS4 replication was due to impairment of progression of cells toward oncosis. Torin-1 treatment significantly reduced the number of oncotic cells at an MOI of 500 at 24 h after infection and at an MOI of 5 and 50 at 48 h after infection (Fig. 7E and F). Torin-1 also reduced the number of SchuS4-GFP-laden cells at 48 h after infection (Fig. 7G to H). An MOI of 500 resulted in a high background GFP signal and too few cells to count at 48 h, and therefore, we could not effectively enumerate oncotic events with infection at this MOI at this time point; consequently, this data set was excluded from the analysis. Similar to the findings obtained by Torin-1 treatment of cells, cyclosporine treatment reduced the number of oncotic and SchuS4-GFP-laden cells at 24 h at an MOI of 500 (Fig. 7E and F). At 48 h after infection, cyclosporine-treated cells had significantly fewer oncotic cells among BMM infected at an MOI of 5 or 50 (Fig. 7E and F). Cyclosporine significantly reduced the number of SchuS4-GFP-laden cells at 24 and 48 h after infection (Fig. 7F). Together, these data demonstrate that Torin-1 and cyclosporine treatment impairs host cell death by temporally blocking SchuS4-induced oncosis, resulting in modest but significant reductions in bacterial loads *in vitro*.

DISCUSSION

Metabolic reprogramming in host macrophages is central to host cell defense against invading pathogens. Generally, upon detection of invading microbes, macrophages shift their metabolic dependence on OXPHOS to glycolysis for generation of ATP and NADH (5). This allows for repurposing of the mitochondria into a multifaceted tool for microbial defense and regulation of inflammation, including the repurposing of tricarboxylic acid cycle intermediates to drive the generation of ROS or antimicrobial metabolites (5, 24). Furthermore, mitochondria are central players in sustaining host cell survival or death (6) and, consequently, control the fate of the replicative niche for intracellular microbes. Therefore, manipulation of mitochondrial function or glycolysis can provide strategic advantages for pathogens (7, 25).

In the case of *F. tularensis* subsp. *tularensis*, prior work demonstrated that the metabolic shift to glycolysis is inhibited in infected macrophages and that this is dependent upon capsule (7). However, it was unclear whether glycolysis was directly inhibited by capsule or whether mitochondrial function was being manipulated. Furthermore, if mitochondrial function was being manipulated, the consequences on cell death pathways were not determined. Data presented herein demonstrate that *F. tularensis* subsp. *tularensis* strain SchuS4 manipulates mitochondrial bioenergetics in

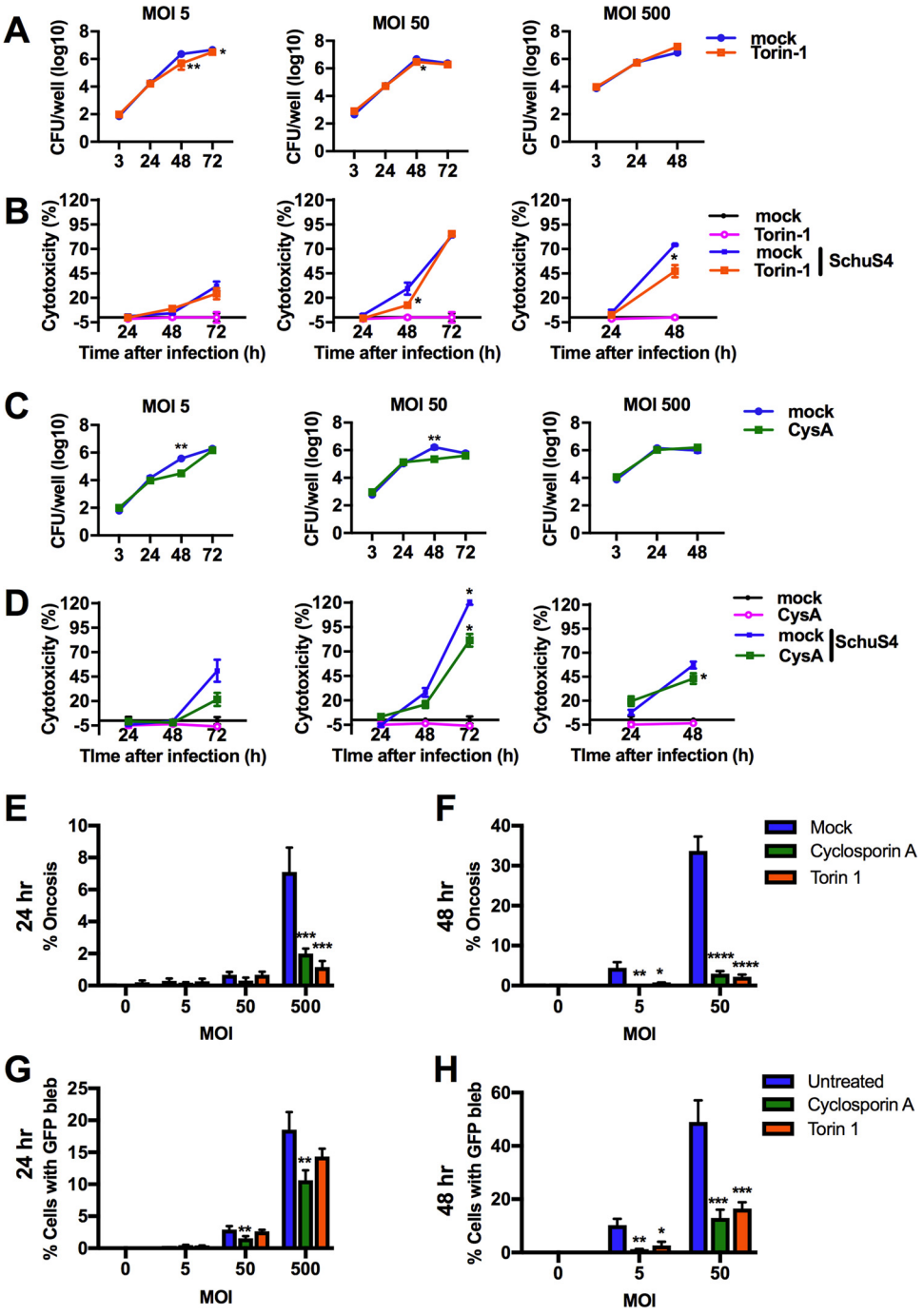

FIG 7 Inhibition of oncosis temporally limits SchuS4 infection. (A) Numbers of CFU in SchuS4-infected BMM (MOI, 5, 50, 500) over time following treatment with Torin-1 (500 nM) or mock treatment (dimethyl sulfoxide). (B) Extracellular LDH activity in supernatants from SchuS4-infected BMM (MOI, 5, 50, 500) over time following treatment with Torin-1 (500 nM) or mock treatment (dimethyl sulfoxide). (C) Numbers of CFU in SchuS4-infected BMM (MOI, 5, 50, 500) over time following treatment with cyclosporine (CysA; 5 μM) or mock treatment (dimethyl sulfoxide). (D) Extracellular LDH activity in supernatants from SchuS4-infected BMM (MOI, 5, 50, 500) over time following treatment with cyclosporine (5 μM) or the vehicle (dimethyl sulfoxide). (E) Percentage of oncotic cells at 24 h following SchuS4 infection (MOI, 5, 50, 500) and treatment with cyclosporine (5 μM), Torin-1 (500 nM), or the vehicle (dimethyl sulfoxide). (F) Percentage of oncotic cells at 48 h following SchuS4 infection (MOI, 5, 50) and treatment with cyclosporine (5 μM), Torin-1 (500 nM), or the vehicle (dimethyl sulfoxide). (G) Percentage of GFP-laden cells at 24 h following SchuS4 infection (MOI, 5, 50, 500) and treatment with cyclosporine (5 μM), Torin-1 (500 nM), or the vehicle (dimethyl sulfoxide). (H) Percentage of GFP-laden cells at 48 h following SchuS4 infection (MOI, 5, 50) and treatment with cyclosporine (5 μM), Torin-1 (500 nM), or the vehicle (dimethyl sulfoxide). Data are presented as the mean ± SEM (for 3 technical replicates) from one representative experiment of three repeats with similar results. *P* values were determined using Student's *t* test for comparison of the numbers of CFU or two-way ANOVA for all other data sets. *, $P < 0.05$; **, $P < 0.01$; ***, $P < 0.001$; ****, $P < 0.0001$.

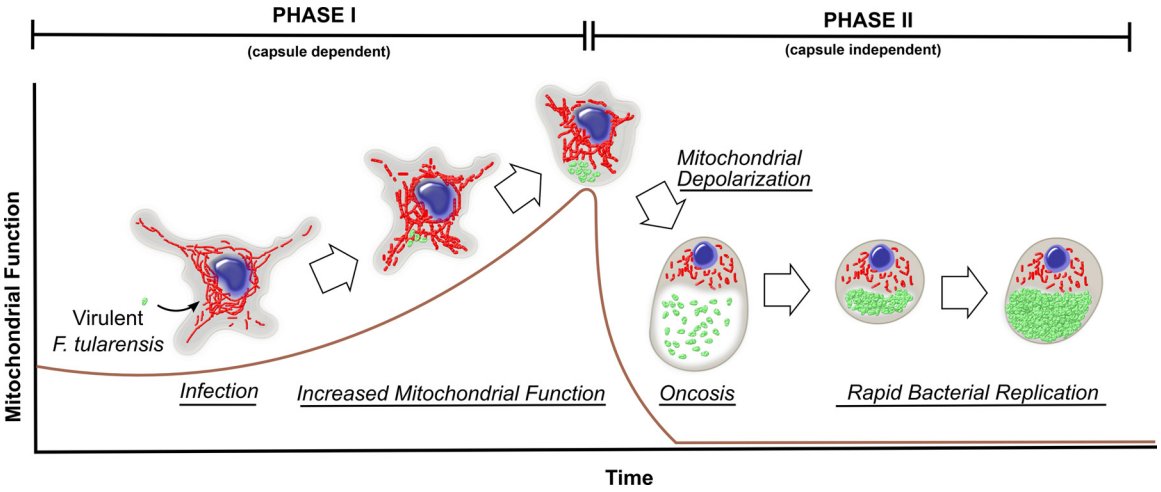

FIG 8 Model of host cell mitochondrial manipulation, bacterial replication, and oncosis in primary macrophages following virulent *F. tularensis* subsp. *tularensis* infection. Virulent *F. tularensis* subsp. *tularensis* facilitated increased mitochondrial function coupled with modest bacterial replication early during infection (phase I). Increased mitochondrial function during phase I was capsule dependent and impaired apoptotic responses. In phase II, *F. tularensis* subsp. *tularensis* infection facilitated a rapid loss in mitochondrial function resulting in oncosis in infected and bystander cells, which was associated with a limited inflammatory response. Oncosis of infected macrophages was paired with a period of rapid bacterial replication within the oncotic blisters.

two phases. Phase I includes increased mitochondrial bioenergetics early during infection (first 8 h) that is capsule dependent and paired with modest bacterial replication. Phase II includes a collapse of mitochondrial function, resulting in oncosis and the rapid replication of bacteria in the intracellular compartment in a process that is not directly dependent upon capsule. Oncosis was the primary form of cell death observed in SchuS4-infected macrophages *in vitro* (see the model presented in Fig. 8).

Capsule-dependent phase I of manipulation of mitochondrial metabolism by *F. tularensis* subsp. *tularensis* specifically involved increased basal OCR and maintenance of the spare respiratory capacity. Improved mitochondrial bioenergetics was due to greater ETC complex I and II activity and a larger mitochondrial network volume. Increased mitochondrial function also promoted production of ATP, which would alleviate or divert the need for the host cell to utilize glycolysis to satisfy energy demands. Decreased spare respiratory capacity can indicate that the mitochondria have the inability to respond to increased ATP demand due to changes in ETC substrate utilization or function and is associated with numerous pathological conditions related to age, stress, inflammation, and cell death (10, 26). Infection with SchuS4 mutants deficient in capsule or strain LVS, as well as treatment with R848 or *K. pneumoniae* capsule, did not result in maintenance of the spare respiratory capacity, which is consistent with a proinflammatory shift linked to impaired mitochondrial function. SchuS4's ability to maintain spare respiratory capacity is likely a central mechanism of virulence that impairs the metabolic shift to glycolysis and the concomitant inflammation.

To our knowledge, this is the first study reporting the ability of a polysaccharide capsule to increase mitochondrial bioenergetics. It is unclear how SchuS4 capsule directly increases mitochondrial metabolism. One possibility is that capsule activates pathways that promote mitochondrial fusion or increase the acquisition of nutrients (such as glutamate and fatty acids) (27–29). Regardless of the specific mechanism, capsule manipulation of mitochondrial function provides a permissive environment within the first 24 h of infection with low bacterial numbers. Given that *F. tularensis* subsp. *tularensis* can cause lethal infections following exposure to as few as 10 bacteria (1), the unique ability of *F. tularensis* subsp. *tularensis* capsule to have this effect on cellular health and the intracellular compartment represents an essential component of virulence for this bacterium.

Mitochondrial manipulation by *F. tularensis* subsp. *tularensis* during phase I resulted

in impaired apoptosis. Activation or impairment of apoptosis following infection with *Francisella tularensis* subsp. *tularensis* is likely variable depending on the cell type or tissue environment. Our results are consistent with reports in which SchuS4 infection delayed apoptosis in human neutrophils (30, 31). However, we found capsule inhibited apoptosis in BMM, which was not evident with human neutrophils (30). Dissimilarity in metabolic programming between neutrophils and BMM, as well as the use of immortalized cell lines which are more glycolytic, could account for observations of apoptosis in SchuS4 infection (30, 32, 33). The presence or absence of apoptosis with SchuS4 infection may also be influenced by the tissue environment *in vivo*. While we did not observe apoptosis *in vitro*, others have reported apoptosis in splenic and liver macrophages *in vivo* following infection with SchuS4 (34). However, apoptosis is not detectable in macrophages in lung tissue of SchuS4-infected mice (2). Therefore, induction of apoptosis may also be dependent upon the tissue environment and the specific metabolic requirements of that tissue or reflect impaired rates of clearance of apoptotic cells within lesions.

We also determined that programmed cell death among BMM is dependent on the strain of *Francisella*. The inability of strain LVS to manipulate host cell bioenergetics, similar to the inability of SchuS4, was anticipated since LVS induces some inflammation early during infection, likely driving decreasing mitochondrial function and steering the host cell fate toward apoptosis and/or necroptosis (14–16, 32, 33, 35). Considering the reported similarities between LVS and SchuS4 capsule (36), differences in mitochondrial manipulation may be surprising. However, to our knowledge, there is no study confirming that the molecular presentations of SchuS4 and LVS capsule are identical or that O antigen is present in a similar abundance. Rather, reports suggest that the O-antigen component of capsule on LVS is associated with core antigen at a ratio higher than that for SchuS4 and/or that it may be less abundant (37, 38). Furthermore, we found that addition of SchuS4 capsule to LVS-infected BMM impaired inflammation and promoted greater intracellular replication of LVS (data not shown). This suggests that any capsule present in LVS is not sufficient to manipulate host cell function and that SchuS4 capsule is more effective at manipulating host inflammation.

The difference between the ability of SchuS4 and LVS to induce inflammation early during infection is likely a key factor in promoting other forms of cell death observed with attenuated strains. For example, consistent with prior observations that described a drop in mitochondrial function in cells infected with attenuated strains of *Francisella*, we observed decreased OCR at the end stage of LVS infection (16). However, in contrast to the findings for SchuS4-infected cells, the timing of these events was key with regard to the outcome of cellular health. SchuS4 mediated a rapid loss in mitochondrial potential, resulting in noninflammatory oncosis, whereas the protracted manipulation of mitochondrial function induced by LVS likely contributes to the inflammatory necroptosis and apoptosis reported by others (16, 32, 33, 35). Thus, identifying the temporal difference in the control of mitochondrial bioenergetics has uncovered the mechanism by which attenuated and virulent strains of *Francisella* progress their host cells to either inflammatory (LVS) or noninflammatory (SchuS4) cell death.

In contrast to the capsule-dependent maintenance of mitochondrial health and cell survival, the capsule-independent phase II in SchuS4-infected BMM was characterized by a rapid drop in cellular ATP levels, $\Delta\Psi_M$, and OCR. Without sufficient ATP reserves, cells can no longer maintain important cellular functions, including maintenance of Na/K^+ ion pumps, leading to a characteristic osmotic swelling of the cell (18). Our data demonstrate that oncosis was the primary form of cell death in *F. tularensis* subsp. *tularensis*-infected macrophages and, importantly, was paired with rapid replication of the bacterium within the last few hours of infection of the primary target cell. The timing and speed by which oncosis occurs are tightly tied to whether the cells will trigger an inflammatory response (21). Rapid mitochondrial failure, induced by depletion of NAD pools, is not associated with the generation of significant inflammation. However, when mitochondrial dysfunction was prolonged (as observed with LVS infection), activation of autophagy and apoptosis occurred,

as did the release of more proinflammatory stimuli, resulting in the establishment of an inflammatory environment (21). The specific oncotic event (cell blistering) in SchuS4-infected BMM occurred rapidly (over the course of 1 to 2 h following a rapid drop in OCR and mitochondrial membrane potential), and this response is consistent with the delay in inflammation observed. Furthermore, rapid oncosis was also observed in bystander cells that did not have bacterial burdens detectable by microscopy. The ability to trigger oncosis in uninfected/low-burden cells may be a strategy employed by SchuS4 to promote a noninflammatory cell death in responding cells that could become activated. Indeed, we have routinely observed a suppression of inflammatory responses among uninfected cells present in SchuS4-infected cultures (39). The mechanism by which oncosis occurs in bystander cells in SchuS4-infected cultures was not clear and is actively being pursued in our laboratory.

Taken together, these studies establish that the manipulation of host mitochondrial metabolism by virulent *F. tularensis* subsp. *tularensis* is a central strategy to limit inflammation and control cell death for optimal bacterial replication. Further understanding of the temporal nature by which host cell metabolism is manipulated during infection with highly virulent pathogens, including but not limited to *F. tularensis* subsp. *tularensis*, could lead to the development of novel antimicrobial treatment strategies. In support of this concept, treatment of *F. tularensis* subsp. *tularensis*-infected BMM with Torin-1 and cyclosporine, which prevent mitochondrial failure in phase II, was effective at reducing oncosis and bacterial replication in these studies. Future studies determining the effectiveness of the blocking of the *F. tularensis* subsp. *tularensis*-mediated increase in mitochondrial function during phase I to control infection are warranted. Collectively, our data support the targeting of mitochondrial function as a therapeutic strategy for *F. tularensis* subsp. *tularensis* infection in future *in vivo* studies, and this study provide an important analysis of the multiple phases of mitochondrial manipulation that may be selectively blocked to control infection.

MATERIALS AND METHODS

Mice and generation of bone marrow-derived macrophages. Female C57BL/6 mice were purchased from The Jackson Laboratory and housed in animal biosafety level 2 facilities at the Rocky Mountain Laboratories. Mice were provided food and water *ad libitum*. All research involving animals was conducted in accordance with Animal Care and Use Committee guidelines that were approved by the Animal Care and Use Committee at the Rocky Mountain Laboratories. Bone morrow-derived macrophages (BMM) were generated using M-CSF (PeproTech, Rocky Hill, NJ) as described in prior work (40).

Bacterial strains. Stock cultures of SchuS4 (Jeannine Peterson, Centers for Disease Control and Prevention, Ft. Collins, CO) and capsule mutant SchuS4 Δ1238 (Bradley Jones, University of Iowa, Iowa City, IA) were generated and used as previously described (39). Genetic complementation of the capsule mutant SchuS4 Δ1238 was accomplished in *trans* by reintroduction through electroporation of a full-length copy of the deleted gene using plasmid pFNLTPomp26 (41). Forward primer 5′-GAGGCTAG CATGAAGCAAGATATATTTCC-3′ and reverse primer 5′-GAGGCTCGAGCTACCCTTGTTTGATCTTTA-3′ were used to amplify *FTT1238c* from SchuS4 genomic DNA to obtain a 1.3-kb product. Following electroporation, bacteria were plated and kanamycin resistance was used to select for successfully complemented colonies. Complementation was verified using the anticapsule antibody MS a-11B7 (Michael Apicella, University of Iowa, Iowa City, IA) at a 1:10,000 dilution (see Fig. S10 in the supplemental material). Avirulent *F. tularensis* subsp. *holarctica* LVS (Karen Elkins, U.S. Food and Drug Administration, Silver Spring, MD) and *F. novicida* strain U112 (Denise Monack, Stanford University School of Medicine, Stanford, CA) were generated and used similarly to the virulent strains. All experiments were performed under approved biosafety level 3 protocols at Rocky Mountain Laboratories.

Purification of *F. tularensis* subsp. *tularensis* capsule. Capsule was isolated and purified from *F. tularensis* subsp. *tularensis* as previously described (7, 36). Briefly, *F. tularensis* subsp. *tularensis* was grown on modified Mueller-Hinton (MMH) agar plates and collected in tubes containing 6 mM Tris, 10 mM EDTA, and 3% (wt/vol) SDS at pH 6.8. Tubes with bacterial isolates were incubated for 24 h at 65°C, followed by addition of 50 μg/ml proteinase K (Thermo Fisher Scientific, Waltham, MA). Bacterial isolates were then incubated for an additional 24 h at 37°C. SDS was removed by ethanol precipitation, and samples were centrifuged at 12,000 $\times$ *g* at 4°C. The resulting pellets were resuspended in 10 mM Tris base with 10 mM $CaCl_2$ (pH 7.4) containing 80 U micrococcal nuclease (Thermo Fisher). Samples were incubated for an additional 24 h and then hot phenol extracted at 65°C for 30 min. Samples were then cooled on ice and centrifuged at 2,000 $\times$ *g* for 10 min at 4°C. The aqueous layer was collected, and the residual phenol layer was back extracted with deionized water. The aqueous layers were then combined, and the phenol was removed via ethanol precipitation. The pellet was then resuspended in high-

performance liquid chromatography-grade water containing 5% (vol/vol) Triton X-114 and incubated at 4°C for 24 h, followed by an additional incubation at 37°C for 1 h. Samples were then centrifuged at 2,000 × *g* for 10 min, and the aqueous phase containing capsule was collected and then lyophilized. Prior to assay, lyophilized capsule was resuspended in sterile tissue culture-grade water.

Purification of *Klebsiella pneumoniae* capsule. *Klebsiella pneumoniae* capsule was generously provided by Frank DeLeo (Rocky Mountain Laboratories, Hamilton, MT). *Klebsiella pneumoniae* was grown from a frozen stock in HYEM medium (2% Hycase-SF, 0.3% yeast extract, 2% maltose) at 37°C with shaking (100 rpm) for 16 h. Bacteria were removed from the cultures by centrifugation at 8,000 × *g* for 30 min. Culture supernatants were then passed through a 0.45-μm-pore-size nylon filter to remove any remaining cells. A 10% stock of *N*-acetyl-*N*,*N*,*N*-trimethylammonium bromide (CTAB; Millipore-Sigma, St. Louis, MO) was added to the supernatants to achieve a final concentration of 0.5% (vol/vol). Supernatants were then incubated at room temperature with stirring for 30 min. The precipitate was then collected by centrifugation (4,200 × *g* for 30 min). The pellet was then dissolved in 1 M $CaCl_2$. Ethanol was added to precipitate the capsule material. The crude capsule material was then treated with proteinase K (100 μg/ml) for 2 h at 37°C. Proteinase K was inactivated by heat denaturing (75°C for 30 min). Samples were cooled back down to 37°C and treated with RNase and DNase (100 μg/ml each; Thermo Fisher) for 2 h at 37°C. RNase and DNase were then deactivated by heat denaturing (75°C for 30 min). Finally, *K. pneumoniae* capsule was treated with polymyxin B (100 μg/ml; Thermo Fisher) for 2 h. Polymyxin B was also added with the capsule to BMM (100 μg/ml) to inhibit residual lipopolysaccharide (LPS) activity.

Infection of BMM for analysis of mitochondrial function. BMM were seeded at a density of 80,000 cells per well in 80 μl complete Dulbecco modified Eagle medium (cDMEM; Dulbecco modified Eagle medium [DMEM] supplemented with glutamine, HEPES, nonessential amino acids, and 10% fetal bovine serum [FBS]) in a 96-well Seahorse bioanalyzer tissue culture plate (Agilent Technologies, Santa Clara, CA) and incubated overnight at 37°C. The SchuS4, Δ1238, or LVS inoculum was prepared from frozen stocks at 5 times the target MOI (MOI, 50) in cDMEM. Capsule was also prepared at 5 times the target concentration (10 μg/ml) in cDMEM. BMM were then infected or treated with capsule by adding 20 μl of the 5× inoculum to the 80-μl well volume to achieve the target MOI or capsule concentration. Infected or capsule-treated BMM were then incubated for the designated times.

Mitochondrial function assay (whole cell). At 1 h prior to analysis of the mitochondrial function of infected or capsule-treated cells, cDMEM was removed, leaving 40 μl of residual volume, and the BMM were washed 2 times with 200 μl of Seahorse Mito Stress medium (DMEM with 25 mM glucose, 2 mM sodium pyruvate, and 2 mM L-glutamine; Agilent Technologies). Next, 140 μl of assay medium was added to each well to make the final well volume 180 μl. Cells were then incubated for 1 h at 37°C in a non-CO_2 incubator. Mitochondrial function was then assessed on a Seahorse XFe96 bioanalyzer (Agilent Technologies) in real time following injection of oligomycin (1.5 μM), carbonyl cyanide-*p*-trifluoromethoxyphenylhydrazone (FCCP; 2.0 μM), antimycin (0.5 μM), and rotenone (0.5 μM) following the manufacturer's standard instructions. Specific mitochondrial parameters were obtained according to calculations described in Fig. S2.

Mitochondrial function assay (permeabilized cells). BMM were prepared and infected (MOI, 50) or treated with capsule (10 μg/ml) and incubated for 6 h as described above. Mitochondrial function was then assessed using methods adapted from those reported by others (9). Immediately prior to the assay, all cDMEM except for 40 μl of residual volume was removed, and the cells were washed once with 300 μl of 1× MAS buffer (220 mM mannitol, 70 mM sucrose, 10 mM KH_2PO_4, 5 mM $MgCl_2$, 2 mM HEPES, 1 mM EGTA, pH 7.2, plus 0.2% [wt/vol] fatty acid-free bovine serum albumin [BSA]). MAS buffer (1×) containing the plasma membrane permeabilizer reagent (1 nM; Agilent Technologies), ADP (4 mM, Millipore-Sigma), and complex I- or complex II-specific substrates was added to the washed wells to achieve a final volume of 180 μl. For complex I substrate utilization, 1× MAS buffer contained glutamate-malate (10 mM and 10 mM, respectively), palmitoyl-L-carnitine–octanyl-L-carnitine–malate (40 μM, 40 μM, and 1 mM, respectively), or pyruvate-malate (10 mM and 1 mM, respectively). For complex II substrate utilization, 1× MAS buffer contained succinate-rotenone (10 mM and 2 μM, respectively). The plates were immediately placed on the Seahorse XFe96 bioanalyzer, and mitochondrial function was assessed using mix, wait, and measure times of 0.5 min, 0.5 min, and 2 min, respectively. No non-CO_2 incubation period or instrument equilibration steps were done prior to the start of the assay to minimize the time that the permeabilized cells were in nonionic medium. Three basal (state 3) measurements of OCR were obtained, and then oligomycin was injected (1.5 μM) to induce state 4o. Three consecutive measurements of the state 4o OCR were obtained. The respiratory control ratio (RCR) was calculated as the mean of the state 3 OCR divided by the mean of the state 4o OCR.

Real-time XFe96 bioanalyzer analysis of basal respiration over time. BMM were washed, and the medium was replaced with Seahorse Mito Stress medium containing mock-infected, SchuS4-infected (MOI, 50), or LVS-infected (MOI, 50) cells. BMM were incubated for 1 h in a non-CO_2 incubator at 37°C and then analyzed on a Seahorse XFe96 bioanalyzer. The basal OCR was assessed every 5 min for a minimum of 12 h.

OCR analysis of bacteria only. The Seahorse XFe96 bioanalyzer was used to assess the OCR of SchuS4 using methods adapted from those of Lobritz et al. (8). Seahorse XFe96 bioanalyzer 96-well tissue culture plates were coated with poly-D-lysine (0.1 mg/ml; Millipore-Sigma) for 30 min at 37°C. Seahorse tissue culture plates were then washed with sterile water and air dried for 1 h. Increasing numbers of SchuS4 were prepared in Seahorse Mito Stress medium or modified Mueller-Hinton (MMH) broth (supplemented with 10% [vol/vol] glucose, 2.5% [vol/vol] ferric pyrophosphate, 10% [vol/vol] IsoVitaleX [Thermo Fisher]). One hundred microliters of bacteria was then added to the Seahorse XFe96 bioanalyzer tissue culture plate and centrifuged at 1,400 × *g* for 10 min to pellet them to the bottom of the tissue

culture plate. The plates were immediately placed on the Seahorse bioanalyzer, and OCR were assessed using mix, wait, and measure times of 3 min, 0.5 min, and 3 min, respectively, for 5 cycles.

Infection of BMM for analysis of cytotoxicity, numbers of CFU, and oncosis. BMM were infected with SchuS4 or LVS as previously described using gentamicin protection (40). Briefly, bacteria were resuspended at an MOI of 5, 50, or 500 in complete DMEM (cDMEM; DMEM supplemented with glutamine, HEPES, nonessential amino acids, and 10% FBS). The medium was removed from BMM (reserve medium), and the inoculum at the MOI designated above and in the figure legends was added to the BMM in a 200-μl final volume. BMM were incubated with the bacteria for 90 min, after which the inoculum was removed and gentamicin (50 μg/ml; Thermo Fisher) was added to the cells for 45 min to eliminate the remaining extracellular bacteria. Gentamicin was then removed, the cells were washed 3 times with phosphate-buffered saline (PBS), and then the reserved medium was added back to the cultures. Where indicated, cells were pretreated with cyclosporine (5 μM; R&D Systems, Minneapolis, MN), Torin-1 (500 nM; R&D Systems), or necrostatin-1 (50 μM; R&D Systems) for 2 h, and the drugs were maintained in the culture throughout the infection. Rotenone (8 μM; Millipore-Sigma) was added to BMM immediately after infection, and cytotoxicity was assessed after 24 h. For studies in which apoptosis was induced by M-CSF depletion, BMM were infected as described above. M-CSF was routinely added after 24 h of infection but was left out for the M-CSF-depleted groups. Cytotoxicity was assessed 24 h later. Intracellular bacteria were enumerated by lysing the cells in distilled water, after which the lysates were serially diluted and plated on MMH agar.

Cytokines, cytotoxicity, and cell permeability assays. IL-12p40 was assessed in cell culture supernatants at 24, 48, and 72 h using a commercially available enzyme-linked immunosorbent assay (BD Biosciences, San Jose, CA). Extracellular lactate dehydrogenase (LDH) activity was used as a marker of cytotoxicity and was measured using a CytoTox 96 nonradioactive cytotoxicity assay according to the manufacturer's instructions (Promega, Madison, WI). Cell permeability was measured using the NucGreen Dead 488 ReadyProbes reagent (Thermo Fisher; excitation wavelength, 504 nm; emission wavelength, 523 nm) and an EVOS FL Auto 2 imaging system (Thermo Fisher). Briefly, 1 drop of the NucGreen reagent was added to each well, and the cultures were incubated for 15 min at 37°C. Cell nuclei were counterstained using the NucBlue Fixed Cell ReadyProbes reagent (excitation wavelength, 360 nm; emission wavelength, 460 nm; Thermo Fisher) and incubated for 5 min at 37°C. Six consecutive fields were imaged per well at a $\times$10 magnification for both the DAPI (4′,6-diamidino-2-phenylindole) and GFP channels and stitched together to form a larger tiled image. Total NucGreen-positive cells and NucBlue-positive cells within the tiled image were counted using ImageJ software. A minimum of 4,000 NucBlue-positive cells were counted per stitched image to generate the percentage of total permeabilized cells.

ATP quantification. Cellular ATP levels were quantified using the mitochondrial ToxGlo reagent according to the manufacturer's instructions (Promega). Briefly, BMM were plated at 40,000 cells/well in a 96-well tissue culture plate and incubated overnight at 37°C in cDMEM. The cDMEM was then removed and saved (reserve medium), and 50 μl of the SchuS4 inoculum (MOI, 5 and 50 in cDMEM) was added to the cells. The cells were incubated for 90 min, and then the inoculum was removed and 100 μl of cDMEM containing gentamicin (50 μg/ml) was added to each well. The cells were incubated with gentamicin for 45 min, and then the gentamicin was removed. The cells were carefully washed 3 times with PBS, and the reserve medium was added back to the infected cells. At the assay time points, the cDMEM was removed and the cells were washed 2 times with serum-free galactose-containing DMEM (gDMEM plus nonessential amino acids, HEPES, L-glutamine, and 100 mM glutamate). One hundred microliters of serum-free gDMEM was then added to the cells. Oligomycin (60 ng/ml; Cayman Chemical, Ann Arbor, MI) was used as the positive control for ATP inhibition and was added to the cells 90 min prior to the reading of the assay results on a plate reader. The plates were equilibrated to room temperature in the dark, and 100 μl of ATP detection reagent was added to each well. Luminescence was then quantified on a GloMax multidetection system (Promega).

Quantification of oncotic and GFP-SchuS4-laden cells. Oncotic cells were quantified using live cell imaging. Briefly, cells in 48-well plates were infected with GFP-SchuS4 (MOI, 5, 50, and 500, as described above using gentamicin protection) and incubated for 24 and 48 h. Using an EVOS FL Auto 2 imaging system and transwell illumination, the oncotic cells in 6 consecutive fields per well were manually counted at a $\times$40 magnification. GFP-SchuS4-laden cells in the same corresponding fields were also manually counted in the GFP channel. In the same fields in which oncotic and GFP-positive cells were manually counted, cells were counterstained with the NucBlue reagent and imaged. The number of nuclei was quantified using ImageJ software, and the corresponding percentage of oncotic or GFP-SchuS4-laden cells was calculated as a percentage of the total number of DAPI-positive cells counted. A minimum of 200 DAPI-positive cells were counted per well.

Western blotting. At the indicated time points, cDMEM was removed from the BMM and the cells were lysed in 150 μl 1$\times$ cell lysis buffer supplemented with phenylmethylsulfonyl fluoride (1 mM; Millipore-Sigma). Lysates were added to NuPAGE lithium dodecyl sulfate (LDS) sample buffer (Thermo Fisher) and heated at 95°C for 10 min. Samples were homogenized by centrifugation using a QIAshredder homogenizer (Qiagen, Hilden, Germany) and loaded onto 4 to 12% SDS-NuPAGE gradient gels (Thermo Fisher). After electrophoresis, proteins were transferred to polyvinylidene difluoride membranes and blocked with 5% BSA in Tris-buffered saline with Tween 20 prior to detection of target proteins. Rabbit polyclonal anti-mouse immunoglobulin antibodies to cytochrome *c*, caspase-9, cleaved caspase-9 (Asp353), caspase-3, cleaved caspase-3 (Asp175), phospho-S6 ribosomal protein (Ser235/236), MLKL (D6W1K), phospho-MLKL, and phospho-RIP (Ser166) were used for detection. Rabbit monoclonal antibodies anti-mouse RIPK (D94C12) and β-actin (13E5) were used to detect total RIPK and β-actin, respectively.

MitoTracker Red staining. BMM were plated on 12-mm glass coverslips in a 24-well plate and infected or treated with capsule (10 μg/ml) following the protocols described for assessment of mitochondrial function. After 6 h, the cDMEM was then aspirated from each well and the cells were washed once with 1 ml Dulbecco's PBS (dPBS). MitoTracker Red CMXRos (50 nM in dPBS; Thermo Fisher) was added to each well, and the plates were incubated at 37°C in the dark for 25 min. Following incubation, the MitoTracker Red solution was aspirated and each well was washed 2 times with 1 ml of dPBS. The cells were fixed with 3% paraformaldehyde in dPBS for 30 min at room temperature in the dark and then washed 3 times with dPBS. Samples were permeabilized and blocked by inversion on 40 μl of 0.3% Triton X-100, 10% horse serum in dPBS for 15 min at room temperature. Cells were labeled by inversion on 40 μl of antibody or stain in 0.3% Triton X-100, 10% horse serum in dPBS for 30 min at room temperature, followed by 3 washes in dPBS. *F. tularensis* subsp. *tularensis* was detected with primary anti-LPS antibody (U.S. Biological, Salem, MA) and then Alexa Fluor 488-conjugated goat anti-mouse IgG (1:1,000; Thermo Fisher). All cells were stained with DAPI (0.02 μg/ml; Thermo Fisher) for 15 min before washing 3 times in dPBS. Cells were washed a further 2 times in water, wicked until dry, and mounted overnight in 5 μl of Mowiol 4-88 mounting medium (Millipore-Sigma). Samples were imaged using a Zeiss LSM 880 microscope with an Airyscan scanner using a 63× objective (Zeiss Micro Imaging, Jena, Germany). z-stack images, each of which was 1,024 by 1,024 pixels, were acquired across the entire depth of each field with a 0.016-μm spacing, and subsequently, the Airyscan image was processed using ZEN image acquisition and processing software (Zeiss Micro Imaging). Images were analyzed and prepared for display using Imaris software (Bitplane Software, Concord, MA). Mitochondrial and cytosol volumes were constructed using user-established parameter sets (Table S1). Images for figures were captured in the 3D surpass view in Imaris software.

Live cell imaging of oncosis, mitochondrial membrane potential, and SchuS4-GFP. Cells were plated in 24-well cover glass plates and infected with SchuS4-GFP at an MOI of 50 using the gentamicin infection protocol described above. At 2 h after removal of the gentamicin, TMRE (Thermo Fisher) was added to the cells as a 10× stock to a final concentration of 50 nM. Time-lapse series were acquired using an EVOS FL Auto 2 imaging system, a 40× objective, and an on-stage incubator. The well plate was allowed to equilibrate for 20 min in the on-stage incubator prior to imaging. z-stacks were acquired every 15 min in all channels across the entire depth of the field every 2 μm.

mtDNA PCR. Mock- or SchuS4-infected BMM in 48-well plates were washed and scraped into dPBS at 6 h following infection with SchuS4, as described above for analysis of mitochondrial function. Three wells from each treatment were pooled for each sample. The cells were lysed, and DNA was purified using a QIAamp DNA minikit (Qiagen) per the manufacturer's recommendations. The mtDNA copy number was quantified using a mouse mitochondrial DNA copy number assay kit (Detroit R&D, Detroit, MI) per the manufacturer's recommendations.

Drug effects on bacterial replication. One hundred and 100,000 CFU was resuspended in MMH broth and exposed to increasing doses of Torin-1 or cyclosporine. The cultures were then incubated for 24 h with mixing (600 rpm). After 24 h, the bacterial cultures were serially diluted in PBS and then plated on MMH agar plates for enumeration of the CFU.

Quantification and statistical analysis. Statistical analysis was performed using GraphPad Prism software (version 7.0). A two-tailed Student's *t* test was used for comparisons between two individual groups. For multiple comparisons, one-way or two-way analysis of variance (ANOVA) was used followed by the Tukey posttest for parametric samples. *P* values of <0.05 were considered significant.

SUPPLEMENTAL MATERIAL

Supplemental material for this article may be found at https://doi.org/10.1128/IAI.00044-18.

SUPPLEMENTAL FILE 1, PDF file, 0.1 MB.
SUPPLEMENTAL FILE 2, PDF file, 1.2 MB.
SUPPLEMENTAL FILE 3, DOCX file, 0.1 MB.
SUPPLEMENTAL FILE 4, MP4 file, 18.0 MB.
SUPPLEMENTAL FILE 5, MP4 file, 18.7 MB.
SUPPLEMENTAL FILE 6, MP4 file, 18.6 MB.

ACKNOWLEDGMENTS

We acknowledge Bradley Jones at the University of Iowa for providing the capsule mutant and valuable insight into the generation of the capsule mutant complement. We thank Michael Apicella at the University of Iowa for the anticapsule antibody. We also acknowledge Tregei Starr for valuable insight into immunofluorescence imaging and the 3D reconstruction presented in this work. We thank Robin Ireland and Lydia Roberts for critical review of the experiments described in this report. Finally, we thank Frank DeLeo and Addie Porter for isolating and providing *K. pneumoniae* capsule.

This work was supported by the Intramural Research Program of the National Institutes of Health, National Institute of Allergy and Infectious Diseases.

F.J., B.S., and C.M.B. designed the experiments; F.J., B.S., E.H., R.B., and C.M.B.

performed the experiments; F.J., B.S., and C.M.B. analyzed the data; and F.J., B.S., and C.M.B. wrote the paper.

We declare no competing interests.

REFERENCES

1. Sjostedt A. 2007. Tularemia: history, epidemiology, pathogen physiology, and clinical manifestations. Ann N Y Acad Sci 1105:1–29. https://doi.org/10.1196/annals.1409.009.
2. Bosio CM, Bielefeldt-Ohmann H, Belisle JT. 2007. Active suppression of the pulmonary immune response by *Francisella tularensis* Schu4. J Immunol 178:4538–4547. https://doi.org/10.4049/jimmunol.178.7.4538.
3. Conlan JW, Chen W, Shen H, Webb A, KuoLee R. 2003. Experimental tularemia in mice challenged by aerosol or intradermally with virulent strains of *Francisella tularensis*: bacteriologic and histopathologic studies. Microb Pathog 34:239–248. https://doi.org/10.1016/S0882-4010(03)00046-9.
4. Tarnvik A, Berglund L. 2003. Tularaemia. Eur Respir J 21:361–373. https://doi.org/10.1183/09031936.03.00088903.
5. O'Neill LA, Pearce EJ. 2016. Immunometabolism governs dendritic cell and macrophage function. J Exp Med 213:15–23. https://doi.org/10.1084/jem.20151570.
6. Monlun M, Hyernard C, Blanco P, Lartigue L, Faustin B. 2017. Mitochondria as molecular platforms integrating multiple innate immune signalings. J Mol Biol 429:1–13. https://doi.org/10.1016/j.jmb.2016.10.028.
7. Wyatt EV, Diaz K, Griffin AJ, Rasmussen JA, Crane DD, Jones BD, Bosio CM. 2016. Metabolic reprogramming of host cells by virulent *Francisella tularensis* for optimal replication and modulation of inflammation. J Immunol 196:4227–4236. https://doi.org/10.4049/jimmunol.1502456.
8. Lobritz MA, Belenky P, Porter CB, Gutierrez A, Yang JH, Schwarz EG, Dwyer DJ, Khalil AS, Collins JJ. 2015. Antibiotic efficacy is linked to bacterial cellular respiration. Proc Natl Acad Sci U S A 112:8173–8180. https://doi.org/10.1073/pnas.1509743112.
9. Divakaruni AS, Rogers GW, Murphy AN. 2014. Measuring mitochondrial function in permeabilized cells using the Seahorse XF analyzer or a Clark-type oxygen electrode. Curr Protoc Toxicol 60:25.2.1–25.2.16. https://doi.org/10.1002/0471140856.tx2502s60.
10. Brand MD, Nicholls DG. 2011. Assessing mitochondrial dysfunction in cells. Biochem J 435:297–312. https://doi.org/10.1042/BJ20110162.
11. Youle RJ, van der Bliek AM. 2012. Mitochondrial fission, fusion, and stress. Science 337:1062–1065. https://doi.org/10.1126/science.1219855.
12. Kelley TW, Graham MM, Doseff AI, Pomerantz RW, Lau SM, Ostrowski MC, Franke TF, Marsh CB. 1999. Macrophage colony-stimulating factor promotes cell survival through Akt/protein kinase B. J Biol Chem 274:26393–26398. https://doi.org/10.1074/jbc.274.37.26393.
13. Belhocine K, Monack DM. 2012. Francisella infection triggers activation of the AIM2 inflammasome in murine dendritic cells. Cell Microbiol 14:71–80. https://doi.org/10.1111/j.1462-5822.2011.01700.x.
14. Periasamy S, Le HT, Duffy EB, Chin H, Harton JA. 2016. Inflammasome-independent NLRP3 restriction of a protective early neutrophil response to pulmonary tularemia. PLoS Pathog 12:e1006059. https://doi.org/10.1371/journal.ppat.1006059.
15. Rathinam VA, Jiang Z, Waggoner SN, Sharma S, Cole LE, Waggoner L, Vanaja SK, Monks BG, Ganesan S, Latz E, Hornung V, Vogel SN, Szomolanyi-Tsuda E, Fitzgerald KA. 2010. The AIM2 inflammasome is essential for host defense against cytosolic bacteria and DNA viruses. Nat Immunol 11:395–402. https://doi.org/10.1038/ni.1864.
16. Singh A, Periasamy S, Malik M, Bakshi CS, Stephen L, Ault JG, Mannella CA, Sellati TJ. 2017. Necroptotic debris including damaged mitochondria elicits sepsis-like syndrome during late-phase tularemia. Cell Death Discov 3:17056. https://doi.org/10.1038/cddiscovery.2017.56.
17. Crane DD, Bauler TJ, Wehrly TD, Bosio CM. 2014. Mitochondrial ROS potentiates indirect activation of the AIM2 inflammasome. Front Microbiol 5:438. https://doi.org/10.3389/fmicb.2014.00438.
18. Weerasinghe P, Buja LM. 2012. Oncosis: an important non-apoptotic mode of cell death. Exp Mol Pathol 93:302–308. https://doi.org/10.1016/j.yexmp.2012.09.018.
19. Akimoto M, Hayashi JI, Nakae S, Saito H, Takenaga K. 2016. Interleukin-33 enhances programmed oncosis of ST2L-positive low-metastatic cells in the tumour microenvironment of lung cancer. Cell Death Dis 7:e2057. https://doi.org/10.1038/cddis.2015.418.
20. Webster KA. 2007. Programmed death as a therapeutic target to reduce myocardial infarction. Trends Pharmacol Sci 28:492–499. https://doi.org/10.1016/j.tips.2007.07.004.
21. Del Nagro C, Xiao Y, Rangell L, Reichelt M, O'Brien T. 2014. Depletion of the central metabolite NAD leads to oncosis-mediated cell death. J Biol Chem 289:35182–35192. https://doi.org/10.1074/jbc.M114.580159.
22. Broekemeier KM, Dempsey ME, Pfeiffer DR. 1989. Cyclosporine is a potent inhibitor of the inner membrane permeability transition in liver mitochondria. J Biol Chem 264:7826–7830.
23. Nakagawa T, Shimizu S, Watanabe T, Yamaguchi O, Otsu K, Yamagata H, Inohara H, Kubo T, Tsujimoto Y. 2005. Cyclophilin D-dependent mitochondrial permeability transition regulates some necrotic but not apoptotic cell death. Nature 434:652–658. https://doi.org/10.1038/nature03317.
24. Garaude J, Acin-Perez R, Martinez-Cano S, Enamorado M, Ugolini M, Nistal-Villan E, Hervas-Stubbs S, Pelegrin P, Sander LE, Enriquez JA, Sancho D. 2016. Mitochondrial respiratory-chain adaptations in macrophages contribute to antibacterial host defense. Nat Immunol 17:1037–1045. https://doi.org/10.1038/ni.3509.
25. Olive AJ, Sassetti CM. 2016. Metabolic crosstalk between host and pathogen: sensing, adapting and competing. Nat Rev Microbiol 14:221–234. https://doi.org/10.1038/nrmicro.2016.12.
26. Desler C, Hansen TL, Frederiksen JB, Marcker ML, Singh KK, Juel Rasmussen L. 2012. Is there a link between mitochondrial reserve respiratory capacity and aging? J Aging Res 2012:192503. https://doi.org/10.1155/2012/192503.
27. Bond MR, Hanover JA. 2015. A little sugar goes a long way: the cell biology of O-GlcNAc. J Cell Biol 208:869–880. https://doi.org/10.1083/jcb.201501101.
28. Pekkurnaz G, Trinidad JC, Wang X, Kong D, Schwarz TL. 2014. Glucose regulates mitochondrial motility via Milton modification by O-GlcNAc transferase. Cell 158:54–68. https://doi.org/10.1016/j.cell.2014.06.007.
29. Yi W, Clark PM, Mason DE, Keenan MC, Hill C, Goddard WA. III, Peters EC, Driggers EM, Hsieh-Wilson LC. 2012. Phosphofructokinase 1 glycosylation regulates cell growth and metabolism. Science 337:975–980. https://doi.org/10.1126/science.1222278.
30. Kinkead LC, Whitmore LC, McCracken JM, Fletcher JR, Ketelsen BB, Kaufman JW, Jones BD, Weiss DS, Barker JH, Allen LH. 2018. Bacterial lipoproteins and other factors released by *Francisella tularensis* modulate human neutrophil lifespan: effects of a TLR1 SNP on apoptosis inhibition. Cell Microbiol 20:12795. https://doi.org/10.1111/cmi.12795.
31. McCracken JM, Kinkead LC, McCaffrey RL, Allen LA. 2016. *Francisella tularensis* modulates a distinct subset of regulatory factors and sustains mitochondrial integrity to impair human neutrophil apoptosis. J Innate Immun 8:299–313. https://doi.org/10.1159/000443882.
32. Lai XH, Golovliov I, Sjostedt A. 2001. *Francisella tularensis* induces cytopathogenicity and apoptosis in murine macrophages via a mechanism that requires intracellular bacterial multiplication. Infect Immun 69:4691–4694. https://doi.org/10.1128/IAI.69.7.4691-4694.2001.
33. Lai XH, Sjostedt A. 2003. Delineation of the molecular mechanisms of *Francisella tularensis*-induced apoptosis in murine macrophages. Infect Immun 71:4642–4646. https://doi.org/10.1128/IAI.71.8.4642-4646.2003.
34. Wickstrum JR, Bokhari SM, Fischer JL, Pinson DM, Yeh HW, Horvat RT, Parmely MJ. 2009. *Francisella tularensis* induces extensive caspase-3 activation and apoptotic cell death in the tissues of infected mice. Infect Immun 77:4827–4836. https://doi.org/10.1128/IAI.00246-09.
35. Doyle CR, Pan JA, Mena P, Zong WX, Thanassi DG. 2014. TolC-dependent modulation of host cell death by the *Francisella tularensis* live vaccine strain. Infect Immun 82:2068–2078. https://doi.org/10.1128/IAI.00044-14.
36. Apicella MA, Post DM, Fowler AC, Jones BD, Rasmussen JA, Hunt JR, Imagawa S, Choudhury B, Inzana TJ, Maier TM, Frank DW, Zahrt TC, Chaloner K, Jennings MP, McLendon MK, Gibson BW. 2010. Identification, characterization and immunogenicity of an O-antigen capsular polysaccharide of *Francisella tularensis*. PLoS One 5:e11060. https://doi.org/10.1371/journal.pone.0011060.
37. Wang Q, Shi X, Leymarie N, Madico G, Sharon J, Costello CE, Zaia J. 2011.

A typical preparation of *Francisella tularensis* O-antigen yields a mixture of three types of saccharides. Biochemistry 50:10941–10950. https://doi.org/10.1021/bi201450v.
38. Hood AM. 1977. Virulence factors of *Francisella tularensis*. J Hyg (Lond) 79:47–60. https://doi.org/10.1017/S0022172400052840.
39. Chase JC, Celli J, Bosio CM. 2009. Direct and indirect impairment of human dendritic cell function by virulent *Francisella tularensis* Schu S4. Infect Immun 77:180–195. https://doi.org/10.1128/IAI.00879-08.
40. Griffin AJ, Crane DD, Wehrly TD, Scott DP, Bosio CM. 2013. Alternative activation of macrophages and induction of arginase are not components of pathogenesis mediated by Francisella species. PLoS One 8:e82096. https://doi.org/10.1371/journal.pone.0082096.
41. Wehrly TD, Chong A, Virtaneva K, Sturdevant DE, Child R, Edwards JA, Brouwer D, Nair V, Fischer ER, Wicke L, Curda AJ, Kupko JJ, III, Martens C, Crane DD, Bosio CM, Porcella SF, Celli J. 2009. Intracellular biology and virulence determinants of *Francisella tularensis* revealed by transcriptional profiling inside macrophages. Cell Microbiol 11:1128–1150. https://doi.org/10.1111/j.1462-5822.2009.01316.x.